CASCADING AND MODIFYING NONRADIATIVE ENERGY TRANSFER MECHANISMS IN STRONG COUPLING REGION OF PLASMONS AND EXCITONS IN SEMICONDUCTOR QUANTUM DOTS

A THESIS
SUBMITTED TO THE DEPARTMENT OF ELECTRICAL AND
ELECTRONICS ENGINEERING
AND THE INSTITUTE OF ENGINEERING AND SCIENCES
OF BILKENT UNIVERSITY
IN PARTIAL FULLFILMENT OF THE REQUIREMENTS
FOR THE DEGREE OF
MASTER OF SCIENCE

By
Onur Akın
August 2010

I certify that I have read this thesis and that in my opinion it is fully adequate, in scope and in quality, as a thesis for the degree of Master of Science.

Assoc. Prof. Dr. Hilmi Volkan Demir (Supervisor)

I certify that I have read this thesis and that in my opinion it is fully adequate, in scope and in quality, as a thesis for the degree of Master of Science.

Assist. Prof. Dr. Ali Kemal Okyay

I certify that I have read this thesis and that in my opinion it is fully adequate, in scope and in quality, as a thesis for the degree of Master of Science.

Prof. Dr. Engin Umut Akkaya

Approved for the Institute of Engineering and Sciences:

Prof. Dr. Levent Onural
Director of Institute of Engineering and Sciences

ABSTRACT

CASCADING AND MODIFYING NONRADIATIVE ENERGY TRANSFER MECHANISMS IN STRONG COUPLING REGION OF PLASMONS AND EXCITONS IN SEMICONDUCTOR QUANTUM DOTS

Onur Akin
M.S. in Electrical and Electronics Engineering
Supervisor: Assoc. Prof. Dr. Hilmi Volkan Demir

August 2010

Nonradiative energy transfer finds important applications in nanophotonics and nanobiotechnology including nanoscale optical waveguiding and biological nanosensors. Various fluorophores can take part in such energy transfer interactions in close proximity of each other. Their emission kinetics can be strongly modified and controlled as a result. For example, colloidal semiconductor quantum dots, also known as nanocrystals, have widely been shown to serve as donors and acceptors among themselves or with other fluorescent species to transfer excitation energy nonradiatively. In their close proximity, emission characteristics of such fluorophores can also be altered when coupled with plasmonic structures, e.g., metal nanoparticles. One favored result of these plasmon-exciton interactions is the emission enhancement. In principle it is possible to plasmon-couple acceptor-donor pairs of nonradiative energy transfer to modify their transfer rate. Such plasmon-mediated energy transfer has been demonstrated, where both acceptor-donor pairs are plasmon-coupled. In these cases, however, the resulting plasmon-exciton interactions are not controlled to take place either at the donor site or the acceptor site but at both of the sites. Therefore, it has previously not been possible to identify the coupled interactions. In this thesis, we propose and demonstrate cascaded

plasmonic - nonradiative energy transfer interactions that are controlled by selectively plasmon-coupling either only the donor quantum dots or only the acceptor quantum dots. For that, we designed a novel self-assembly architecture of our hybrid layered systems of semiconductor nanocrystals and metal nanoparticles in a bottom-up fashion through precise spatial and spectral control. This scheme uniquely allowed for the ability to spatially control plasmon-exciton interactions to take place either at the "start" site (donors) or "finish" site (acceptors) of the energy transfer. This control was achieved by placing the plasmonic layer in the right proximity of the donors (for strong donor-exciton plasmon-coupling) while sufficiently being far away from the acceptors (for weak acceptor-exciton plasmon-coupling), or vice versa. Here we comparatively studied and analyzed consequent modifications of quantum dot emission kinetics in response to both cases of plasmon-coupling to only the donors and to only the acceptors through steady-state and time-resolved photoluminescence measurements, along with their lifetime and rate calculations. Such cascaded energy transfer interactions in the strong exciton-plasmon coupling region hold great promise for innovative near-field photonic devices and biological tags.
system.

Keywords: Förster-type non-radiative energy transfer; plasmonics, localized surface plasmons; semiconductor nanocrystals, colloidal quantum dots; gold nanoparticles, metal nanostructures; excitons, spontaneous emission, photoluminescence, plasmon coupled photoluminescence.

ÖZET

YARIİLETKEN KUVANTUM NOKTACIKLARINDA PLAZMON-EKZİTON GÜÇLÜ ETKİLEŞİM ALANINDA IŞINIMSAL OLMAYAN ENERJİ TRANSFER MEKANİZMALARININ SIRALANDIRILMASI VE DEĞİŞTİRİLMESİ

Onur Akın
Elektrik ve Elektronik Mühendisliği Bölümü Yüksek Lisans
Tez Yöneticisi: Doç. Dr. Hilmi Volkan Demir
Ağustos 2010

Işınımsal olmayan enerji transferi nanofotonik ve nanobiyoteknoloji alanlarında, nanoboyutta optik dalga kılavuzu ve biyolojik nanosensör gibi önemli uygulamalarda yer bulmaktadır. Söz konusu yakın mesafeli enerji transfer etkileşimlerinde çeşitli ışıyıcılar kullanılabilmektedir. Bunun sonucunda da ışıma kinetikleri etkili bir şekilde değiştirilebilmektedir ve kontrol edilebilmekteir. Örneğin, nanokristaller olarak da bilinen yarıiletken kuvantum noktacıkları ya kendi aralarında ya da çeşitli ışınır malzemelerle uyarılma enerjilerini aktararak alıcı ya da verici olarak kullanılagelmektedir. Ayrıca, böyle ışıyıcıların ışıma özellikleri metal nanoparçacıklar gibi plazmonik yapılarla yakın mesafelerde etkileşime girdiklerinde değiştirilebilir. Bu plazmon-ekziton etkileşimlerinin önemli sonuçlarından biri de ışımanın güçlendirilmesidir. Kuramsal olarak plazmonik etkileşmeyle alıcı-verici çiftinin ışınımsal olmayan enerji aktarım hızının değiştirilmesi mümkündür. Bu tür plazmon vasıtasıyla yapılan enerji aktarımı her iki alıcı-verici çiftinin de plazmonlara etkileşmesiyle gösterilmiştir. Ancak, meydana gelen plazmon-ekziton etkileşiminin alıcı mı verici mi tarafında olmasının kontrolü her iki

tarafta da olduğu için yapılamamıştır.Bu nedenle, bu etkileşimlerin ayrı ayrı tespiti de mümkün olmamıştır.

Bu tezde, plazmon vasıtasıyla yapılan ışınımsal olmayan enerji transfer etkileşimlerinin seçici bir şekilde ya yalnızca alıcıya kenetlenen plazmonlar ya da yalnızca vericiye kenetlenen plazmonlar olarak sıralandırılmasını öneriyor ve gösteriyoruz. Bu amaçla, melez katmanlı yarıiletken nanokristaller ve metal nanoparçacıklar sistemi için temelden başlayarak kendiliğinden bir araya gelen ve hassas bir şekilde uzaysal ve spektral kontrolü mümkün olan yeni bir mimari tasarladık.

Bu yapı sayesinde plazmon-ekziton etkileşimlerinin enerji aktarımının "başlangıç" (verici) veya "bitiş" (alıcı) tarafında gerçekleşmesinin kontrolü benzersiz bir şekilde mümkün olmuştur. Bu kontrolün sağlanması için plazmonik katman vericiye (güçlü verici ekziton-plazmon kenetlenmesi için) uygun yakınlıkta ve alıcıdan (zayıf alıcı ekziton-plazmon kenetlenmesi için) yeterli uzaklıkta olmalıdır veya tam tersi olmalıdır. Bu noktada, kuvantum noktacıklarının ışıma kinetiği değişimini, plazmonların yalnızca vericiye kenetlenmesi veya plazmonların yalnızca alıcıya kenetlenmesi durumlarına göre durağan durum ve zamanlı çözülüm fotoışıma ölçümleri ve yarı ömür ve hız hesaplamaları kullanarak karşılaştırmalı olarak inceledik ve çalıştık. Bu tür güçlü ekziton-plazmon kenetlenme alanındaki sıralandırılmış enerji aktarımı etkileşimleri yeni nesil yakın-alan fotonik aygıtlarının ve biyolojik elemanlarının geliştirilmesini vaat eder.

Anahtar sözcükler: Förster türü ışınımsal olmayan enerji transferi; plazmonik, bölgesel alan plazmonları; yarıiletken kuvantum noktacıkları, koloidal kuvantum noktacıkları; altın nanoparçacıklar, metal nanoyapılar; ekziton, kendiliğinden ışıma, fotoışıma, plazmon kenetlenmiş ışıma.

Acknowledgements

I would like to thank my supervisor Assoc. Prof. Dr. Hilmi Volkan Demir for his endless support from the beginning of my academic career. Especially, I would like to thank him for his patience and motivation during my loss and grief. I am sure that without his endless support and motivation I would not be able to give this thesis.

I would like to thank Asst. Prof. Dr. Ali Kemal Okyay for his contributions and guidance during my research efforts and also giving useful comments and suggestions as being a member of my thesis jury.

I would like to thank Prof. Dr. Engin Umut Akkaya for his contributions and guidance during my research efforts and also giving useful comments and suggestions as being a member of my thesis jury.

I would like to thank my family Semiha and İsmail Akın for their endless love and support. I would not be able to deal with the hardest era of my life without their presence.

I really want to thank Kazım Gürkan Polat, Mustafa Akın Sefünç and Özgür Kazar, who are my best friends in Bilkent, for their friendship and support. Especially, I would like to thank them for visiting me almost everyday in the hospital while I was recovering from leg injury.

I would like to thank all former and recent group members of Devices and Sensors Group, who work under the supervision of H. Volkan Demir. I would especially like to thank Sedat Nizamoğlu, Rohat Melik, Evren Mutlugün, Can Uran, Özge Özel, Refik Sina Toru, Burak Güzeltürk, Talha Erdem, Sayim Gökyar, Veli Tayfun Kılıç, Emre Ünal, Özgün Akyüz, Emre Sarı, Urartu Şeker and Nihan Koşku Perkgöz.

I would especially like to thank Tuncay Özel for his great guidance and support during the completion of this project.

Lastly, I really want to thank my best friends Murat Ekşi, Oğuz Özlem, Ekin Ağsarlıoğlu, Asım Burak Er and Özgür Soydemir, who are like brothers to me, for their endless friendship, endless support and hospitality all the time.

Table of Contents

ACKNOWLEDGEMENTS VII

INTRODUCTION 1

LOCALIZED SURFACE PLASMON RESONANCE 5

2.1 ELECTRICAL AND OPTICAL PROPERTIES OF METALS 5

2.2 DRUDE MODEL 7

2.3 LOCALIZED SURFACE PLASMONS 8

2.4 MIE THEORY 10

2.5 EMISSION ENHANCEMENT USING LOCALIZED SURFACE PLASMONS 11

2.6 GOLD NANOPARTICLE SYNTHESIS 16

SYNTHESIS AND THIN FILM DEPOSITION OF COLLOIDAL QUANTUM DOTS 19

3.1 SEMİCONDUCTOR QUANTUM DOTS 20

3.2 COLLOIDAL QUANTUM DOT SYNTHESIS IN AQUEOUS MEDIUM 22

3.3 RF CHARACTERİZATİON OF COLLOİDAL QUANTUM DOTS 26

3.4 RF OPTİCAL CHARACTERİZATİON OF COLLOİDAL QUANTUM DOTS 29

3.5 COLLOİDAL QUANTUM DOT THİN FİLM DEPOSİTİON 32

PLASMON MEDIATED NONRADIATIVE ENERGY TRANSFER 35

4.1 PREVİOUS LİTERATURE AND CONTRİBUTİON OF THİS WORK 36

4.2 PREVİOUS LİTERATURE AND CONTRİBUTİON OF THİS WORK 37

4.3 NONRADİATİVE ENERGY TRANSFER USİNG PLASMON EXCİTON COUPLİNG 40

4.4 PLASMON MEDIATED NONRADIATIVE ENERGY TRANSFER BETWEEN QUANTUM DOTS AND METAL NANOPARTICLES 43

4.4.1 PLASMON COUPLING BETWEEN ACCEPTOR QUANTUM DOTS AND METAL NANOPARTICLES.....44
4.4.2 PLASMON COUPLING BETWEEN DONOR QUANTUM DOTS AND METAL NANOPARTICLES.....48
CONCLUSIONS 55

List of Figures

Figure 2. 1 Localized surface plasmons coupled to electromagnetic wave. [18] 9
Figure 2. 2 Resonance frequency shift of our metal nanoparticle solids growing in size. 11
Figure 2. 3 Emission quenching of our CdTe quantum dots very close to metal nanoparticles. 13
Figure 2. 4 Emission enhancement decreasing with increased thickness between our CdTe quantum dots and gold nanoparticles. 14
Figure 2. 5 Coulomb interactions between a metal nanoparticle and fluorescent molecule. 15
Figure 2. 6 AFM pictures of gold nanoparticles of 2 (a) and 5 (b) monolayers. 18

Figure 3. 1 Transmission electron microscope graph of a colloidal quantum dot synthesized at our nanomaterial synthesis laboratory. 20
Figure 3. 2 Illustration of atom stacking CdTe quantum dots from our simulations. 21
Figure 3. 3 Our glove box and experimental synthesis setup in the fume hood. 25

Figure 3. 4 Color variation of our CdTe quantum dots at our nanomaterial synthesis laboratory. 26
Figure 3. 5 (a) TOPO-capped CdSe QD (with only one TOPO ligand shown in the sketch for the sake of clarity) and (b) alignment of QDs when an external bias is applied across the plates of the microfabricated on-chip setup. 27
Figure 3. 6 Dipole moment of TOPO-capped CdSe QDs in different sizes (27 Å, 36 Å, and 53Å) measured as a function of operating frequency by impedance analyzer. 28
Figure 3. 7 Relative permittivity and dipole moment (in the inset) of TOPO-capped CdSe QD (27 Å) measured as a function of operating frequency by programmable network analyzer. 28
Figure 3. 8 Dipole moments of TOPO-capped CdSe core QD (21 Å) and CdSe-ZnS core-shell QD (21.5 Å) measured as a function of operating frequency by programmable network analyzer. 29
Figure 3. 9 Absorption spectra of our CdTe quantum dots of varying size controlled by reaction growth time (from 5 min. to 22 h. 30 min.). 30
Figure 3. 10 Photoluminescence spectra of our CdTe quantum dots of varying size controlled by growth time (from 5 min. to 22 h. 30 min.). 31
Figure 3. 11 Time-resolved fluorescence spectra of our CdTe quantum dots with two different sizes (emitting at 560 and 640 nm peak wavelengths).....32
Figure 3. 12 Deposition of positively and negatively charged layers using layer by layer deposition technique.....33
Figure 3. 13 Steps of layer by layer deposition method.....33

Figure 3. 14 Scanning electron microscop graph of our thin film CdTe quantum dot solids deposited by layer-by-layer assembly technique. 34

Figure 4. 1 Absorbance spectrum of our acceptor quantum dots and emission spectrum of donor quantum dots. 38
Figure 4. 2 Schematic representing the layered architecture of our FRET sample. 39
Figure 4. 3 PL spectra of our donor, acceptor and FRET samples...40
Figure 4. 4 Schematic representing the layered architecture of our plasmon sample. 41
Figure 4. 5 PL spectra of our donor, acceptor, plasmon coupled donor, and plasmon coupled acceptor samples. 42
Figure 4. 6 TRF spectra of our acceptor and plasmon coupled acceptor samples. 42
Figure 4. 7 TRF spectra of our donor and plasmon coupled donor samples. 43
Figure 4. 8 Schematic representing the layered architecture of our plasmon coupled acceptor FRET sample.....45
Figure 4. 9 PL spectra of our acceptor only sample and plasmon coupled acceptor FRET sample.....46
Figure 4. 10 TRF spectra of our donor, FRET, uncoupled donor and plasmon mediated FRET samples. 47
Figure 4. 11 TRF spectra of our acceptor and plasmon mediated FRET samples.....48
Figure 4. 12 Schematic representing the layered architecture of our plasmon coupled donor FRET sample.....49

Figure 4. 13 PL spectra of our donor and plasmon coupled donor FRET samples.....50
Figure 4. 14 TRF spectra of our acceptor and plasmon mediated FRET samples.....51
Figure 4. 15 TRF spectra of our only donor, FRET, uncoupled donor and plasmon mediated FRET samples.....52
Figure 4. 16 TRF spectra of donor, acceptor, FRET and plasmon mediated FRET samples. 53

List of Tables

Table 4. 1 Integrated emission intensities at the peak wavelength of the donor nanocrystals. 53
Table 4. 2 Integrated emission intensities at the peak emission wavelength of the acceptor nanocrystals. 54

For Bestegül Akın, with thanks for being my sister

Chapter 1

Introduction

Over the past two centuries atoms and molecules have been studied by chemists while physical properties of bulk or confined form of materials have been explored by solid-state physicists and material scientists. However, physical properties of materials in the size regime of 1-100 nm have not been as intensively studied until the end of seventies. Following the developments in optical characterization, nanoscale fabrication tools and simulation programs supported by high computation power, researchers have recently found the opportunity of studying new physical phenomena occurring in nanoscale materials. Especially, metal and semiconductor nanoparticles have started attracting the attention of scientists as materials in this size regime, unlike their atomic or bulk form, showed the dependence of their optical and electrical properties on their size and shape as their size becomes comparable to natural length scales of materials [1].

Metal nanoparticles and metal-dielectric surfaces are utilized in the field of plasmonics for localizing and guiding electromagnetic waves at subwavelength dimensions. Plasmonics, almost an hundred years old field, has attracted the attention of researchers from many disciplines including chemistry, material science and engineering since it offers possible applications in a wide range of fields including photonics and biology [2]. Origin of plasmonics goes through ancient Romans, who used metallic nanoparticles in staining of glass. Famous scientists including Mie, Fano and Ritchie had contributed different aspects of this field in the 20th century [3,4,5]. Following the developments in optical characterization and scientific high power computation of silicon technology,

recent research has been conducted on utilization of metallic nanoparticles in fluorescence enhancement, near-field optical spectroscopy and detection. Especially, noble metals play fundamental role in field of optoelectronics as both metal nanoparticles and metal-dielectric hybrid particles such as gold, silver and gold covered by silica shell span the visible part of the electromagnetic spectrum for absorption and near-field localization enhancement [6].

Along with the research conducted on metallic nanoscale materials, optical and electronic properties of semiconductors are also extensively studied over the last few decades [7,8]. Similar to confinement of electromagnetic waves through metallic surfaces, nanoscale semiconductors enabled the higher order confinement of electron-hole pairs in two and three dimensions (quantum wires, quantum dots). This, in addition to one dimensional confinement of quantum wells, so-called quantum size effect leads to discrete energy states and enables tuning of emission color by simply changing the size of the semiconductor material. Synthesis of semiconductor quantum dots began with prototype cadmium sulfide and many different nanocrystals including PbS, ZnS, CdTe have been subsequently synthesized [9]. Also, nanocrystals in various architectures such as core-shell and onion-like structures have also later been synthesized [10]. Size of these nanocrystals is controlled by increasing or decreasing the time of growth. This way a broad range of electromagnetic spectrum starting from near ultraviolet reaching to far infrared is covered by quantum dots of various semiconductors. Besides tuning the emission properties of quantum dots by size variation, solubility of colloidal quantum dots in different media can be controlled and they can be made positively or negatively charged. This surface property can be changed through simple ligand exchange methods. Thus, as a result of these marvelous properties quantum dots have found various important applications in several areas including optics, photonics and biology. Especially, they are extensively used in the field of optoelectronics as embedded parts in light emitting diodes, solar cells and lasers [11, 12].

Förster resonance energy transfer (FRET) is a non-radiative energy transfer mechanism that is extensively used in almost all applications utilizing various species of fluorescent molecules [13]. Since semiconductor quantum dots are also fluorescent molecules, FRET mechanism can be realized between different sized quantum dots in close proximity for emission enhancement. This process starts with excitation of one of the quantum dots (donor) and is followed by nonradiative energy transfer to the other quantum dot (acceptor) since the transition dipole moments of this pair is coupled. Energy transfer efficiency and rate between these particles depend on several factors including spectral overlap between absorption spectrum of the acceptor quantum dots and emission spectrum of the donor quantum dots and quantum efficiency of quantum dots. Therefore, recent research is done on accelerating the energy transfer rate between these quantum dots by optimizing the conditions [14].

Another important non-radiative energy transfer mechanism plasmon coupling which enhances the emission of quantum dots by means of re-transferred excitation energy between quantum dots and metal nanoparticles. This process also depends on several factors including spectral overlap, with most critical parameter being the distance between these particles. Depending on this distance, emission of quantum dot can either be quenched or enhanced or completely uninfluenced if they are too far away. Recent research has been carried out on combining these energy transfer mechanisms of FRET and plasmon coupling in a constructive way to further enhance emission and fasten the rate of energy transfer [15, 16]. However these previous studies only included that cases of plasmon coupling to both the donor-acceptor quantum dots of the FRET pair. For this purpose, thin films of quantum dot and metal layers are fabricated in different structures or hybrid metal and hybrid quantum dots are used. For the first time in thesis, we proposed and developed layered architectures that allow for selective plasmon coupling only to the component of the FRET pair, but not to both, through spatial control.

In this thesis work, we systematically studied the emission and energy transfer characteristics of complex structures composed of metal nanoparticles and quantum dots placed in a distance controlled way. We fabricated our samples using layer by layer deposition technique. Using these samples we observed and identified the effects of plasmon and FRET resonance energy transfers separately.

This thesis is organized as follows. In Chapter 1, both general properties of metal and semiconductor nanoscale materials and nonradiative energy mechanisms are shortly discussed. Recent research work on nonradiative energy transfer confined with plasmon coupling is briefly discussed and finally our approach to the problem of cascaded energy transfer mechanism with selective plasmon coupling is given. In Chapter 2, electromagnetics of metals at nanoscale is explained in detail. Localized surface plasmons and their dependence on various conditions are elaborated and furthermore their utilization in emission enhancement is described. Finally, metal nanoparticle synthesis procedure is provided. In Chapter 3, a brief introduction on semiconductor quantum dots is given and optical and electrical properties of these particles are discussed. CdTe quantum dot synthesis procedure and optical characterization of these dots are presented. Finally, layer by layer deposition method is discussed in detail. In chapter 4, first plasmon coupled and Förster resonance energy transfer mechanisms are discussed through data analysis of our gold nanoparticle and CdTe nanocrystal samples. Plasmon mediated energy transfer is further discussed for two cases of plasmon coupling to the acceptor nanocrystals only and plasmon coupling to the donor nanocrystals only. In chapter 5, the thesis work is summarized and a possible future perspective is given.

Chapter 2

Localized Surface Plasmon Resonance

2.1 Electrical and Optical Properties of Metals

Materials are grouped into three depending on their degree of electrical conductivity: insulators (dielectrics), conductors and semiconductors. Electrons are included as bounded charges in dielectric media, whereas they are free and can wander through the surface of the conducting media. When an electromagnetic field is applied to a dielectric medium, a fundamental result of the interaction of electromagnetic field with bounded charges is the polarization of the medium due to creation of electric dipoles. An eminent property of conducting materials exposed to electromagnetic fields is however, the creation of current flow.

Metals are very good conductors of electricity. Especially, gold and silver have static conductivities in the range of 10^7 - 10^8 Siemens per meter, while good insulators such as porcelain and glass have static conductivities in the range of 10^{-12} - 10^{-14} Siemens per meter [17]. Free electrons of metals are also responsible for high reflectivity and absorptivity of metals up to the visible frequencies. These properties of metals enable their utilization as cladding layers of waveguides and resonators for propagation of electromagnetic waves in electrical engineering. However, when the frequency of the external electromagnetic field reaches to far infrared region of the electromagnetic spectrum, both penetrating field inside the metal and dissipation increase. As the frequency of the applied field is further increased to ultraviolet region of the electromagnetic spectrum,

then the metal starts to behave as if it is a dielectric material and allows the transmission of the electromagnetic field through it.

Noble metals such as gold and silver are exceptions to this case since electronic band transitions in this frequency regime lead to the absorption of the incident field through the material. This frequency dependent response of materials to the external electromagnetic field is explained theoretically in terms of intrinsic properties of the material medium such as permittivity and conductivity. Assuming a linear, isotropic and nonmagnetic medium, the internal current density is related to the external field via conductivity of the medium while the polarization vector is related to the external field via susceptibility, which is directly related to permittivity of the medium for external fields of low frequencies. Thus, the conductivity represents the contribution of free electrons to the response of the medium and the susceptibility stands for the response of the bound charges to the external stimuli.

As the frequency of the external field is increased, response of both free and bound charges may not always follow the rapidly changing field, especially when the frequency of the applied field reaches the reciprocal of the electron relaxation lifetime of the material. Thus, the discrepancies between bound and free charges become uncertain for high frequencies of external electromagnetic field where conductivity and permittivity become related. Using the relations between internal current density and polarization in constitutive relations of material media, the relation between conductivity and permittivity can be derived as in (2.1) as a function of the wavelength of electromagnetic field longer than all the characteristic dimensions of the material:

$$\varepsilon(\omega) = \varepsilon_{\infty} + \frac{i\,\sigma(\omega)}{\varepsilon_0\,\omega} \tag{2.1}$$

As can be seen from (2.1), permittivity of the material medium, ε(w) is represented as a complex quantity. Imaginary part of the permittivity stands for

absorption of the incoming field while real part of the permittivity is counted for refractive index of the medium.

2.2 Drude Model

Following the discovery of electron in 1897, Paul Drude applied kinetic theory of gasses to metals as if they are gasses of electrons. Drude considered the electrons as uniform solid spheres that move in straight lines under the influence of an external electromagnetic field (free electron approximation). These uniform solid spheres were also assumed to keep moving until they collide and change their velocity abruptly after a certain time, which is known as relaxation time (independent electron approximation) [18].

One of the successful applications of Drude model is the derivation of complex conductivity that can be used to explain AC conductivity of metals. This frequency dependent conductivity is given in (2.2) as the equation of motion per momentum of electron is solved.

$$\sigma(w) = \frac{\sigma_0}{1 - iw\tau} \tag{2.2}$$

Relative permittivity of metallic medium can also be derived by applying Maxwell's equations and using the relation between internal current density and applied electric field given by Drude model. Then, the relative permittivity of metallic medium is found in (2.3):

$$\varepsilon(w) = 1 - \frac{w_p^{\ 2}}{w^2} \tag{2.3}$$

where w_p is the plasma frequency of the material. For frequencies smaller than w_p, permittivity of the medium is negative and complex, which leads to absorption and reflection of incoming field depending on how close the frequency of the incoming field is to the plasma frequency of the metal. However, when the frequency of the incoming field exceeds the plasma frequency,

permittivity of the medium becomes positive which allows the propagation of the incoming field through the metal. Several alkali metals such as sodium and potassium become transparent for ultraviolet frequencies, which exceed their plasma frequencies.

Finally, when the frequency of the external electromagnetic field is equal to the plasma frequency of the metal, electric field behaves as a solely depolarization field and the gas of free electrons (metal's free electrons) starts to oscillate longitudinally with respect to positive ion cores analogous to a driven oscillator. These quanta of oscillations of the gas of free electrons are called plasmons.

2.3 Localized Surface Plasmons

The longitudinal oscillations of free electrons of metals can also be defined as volume plasmons to distinguish them from surface plasmon polaritons and localized surface plasmons. Surface plasmon polaritons are traveling electromagnetic waves that are excited along the interface of a metal and a dielectric material. However, localized surface plasmons are non-propagating coherent oscillations of free electrons of metal nanoparticles excited via electromagnetic coupling.

Electromagnetic waves acting on a metal nanoparticle force the free electrons of this particle to be displaced relative to its center. Then a restoring force acts on these free electrons. This interaction leads to oscillation of the electron cloud as illustrated in Figure 2.1.

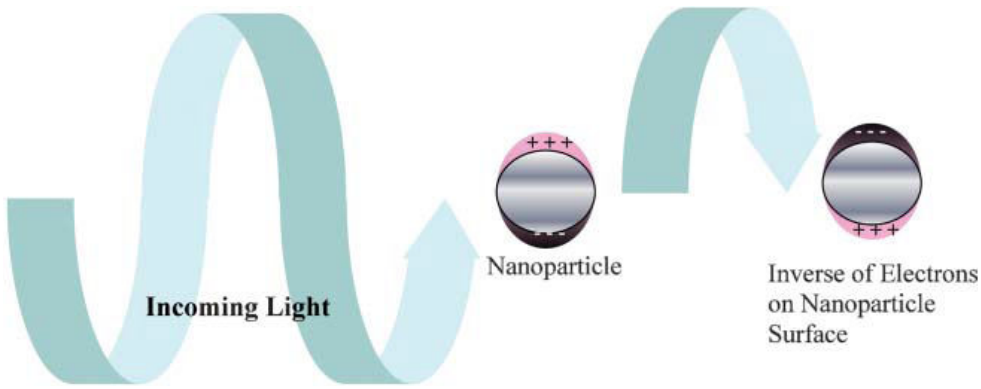

Figure 2. 1 Localized surface plasmons coupled to electromagnetic wave [18].

The excitation of localized surface plasmons is generally achieved via electromagnetic waves of wavelengths that are much longer than the spatial dimensions of the target metal nanoparticle. Therefore, the spatial variation of the electric field inside and around the particle is almost zero. Thus electric field calculations inside and around this particle can be performed using electrostatic Maxwell's equations instead of electrodynamics. This treatment is called quasi-static approximation [19]. In this approach, Laplace's electric potential equation is solved for a uniform sphere that interacts with a static electric field. After applying appropriate boundary conditions such as the continuity of the dielectric displacement vector and electric potential, the functions of electric potential inside and outside the sphere are derived as in (2.4) and (2.5).

$$\phi_{in} = \frac{3\varepsilon_m}{\varepsilon + 2\varepsilon_m} E_0 r \cos\theta \tag{2.4}$$

$$\phi_{out} = -E_0 r \cos\theta + \frac{\varepsilon - \varepsilon_m}{\varepsilon + 2\varepsilon_m} E_0 a^3 \frac{\cos\theta}{r^2} \tag{2.5}$$

where ε_m is the dielectric constant of the metal nanoparticle, ε is the dielectric constant of the surrounding medium, E_0 is the magnitude of the external electromagnetic field, θ is the angle between the applied field and the scattered field from the sphere, and r is the distance to the center of the metal nanoparticle.

As can be clearly seen from (2.4) and (2.5) , resonance occurs for so called Fröhlich condition where the real part of the dielectric constant of metal

nanoparticle is equal to minus half of the dielectric constant of the surrounding medium. Since the dielectric constant of the metal nanoparticle is frequency dependent, Fröhlich condition can be achieved for certain electromagnetic fields. When Fröhlich condition is satisfied, both the electric fields inside and outside the metal nanoparticle are amplified with respect to the external electromagnetic field.

It is obvious that Fröhlich condition depends on both the dielectric constant of metal nanoparticle and dielectric constant of the surrounding medium. Therefore, as the dielectric constant of the surrounding medium increases, resonance frequency of the nanoparticle shifts to red.

Although environment dependency of resonance frequency of metal nanoparticles can be easily extracted from (2.4) and (2.5), it is also experimentally found that the peak wavelength and bandwidth of resonance depend both on the shape and size of metal nanoparticles. For, small sized metal nanoparticles whose diameter is smaller than 20 nanometers (2.4) and (2.5) should be modified to include the effect of surface electron scattering since electron mean free path of metal nanoparticles such as in gold and silver is on the order of tens of nanometers. When this effect is also considered, it is found that plasmon bandwidth of the metal nanoparticles decreases as the radius of the nanoparticle increases.

2.4 Mie Theory

Throughout the derivation of localized surface plasmon resonance, electrostatic equations are used instead of electrodynamics due to validity of quasi-static approximation. However, for the derivation of the resonance condition of metal nanoparticles that have diameters greater than 30 nanometers, electrostatic equations cannot be used since quasi-static approximation is no longer valid. In this region of size, Mie theory should be used to derive the equations of absorption and scattering for obtaining the absorption spectra and resonance

frequency [20]. Figure 2.3 shows the resonance frequency shift of our Au NPs deposited in increasing number of MLs, while effectively growing in size as metals solids.

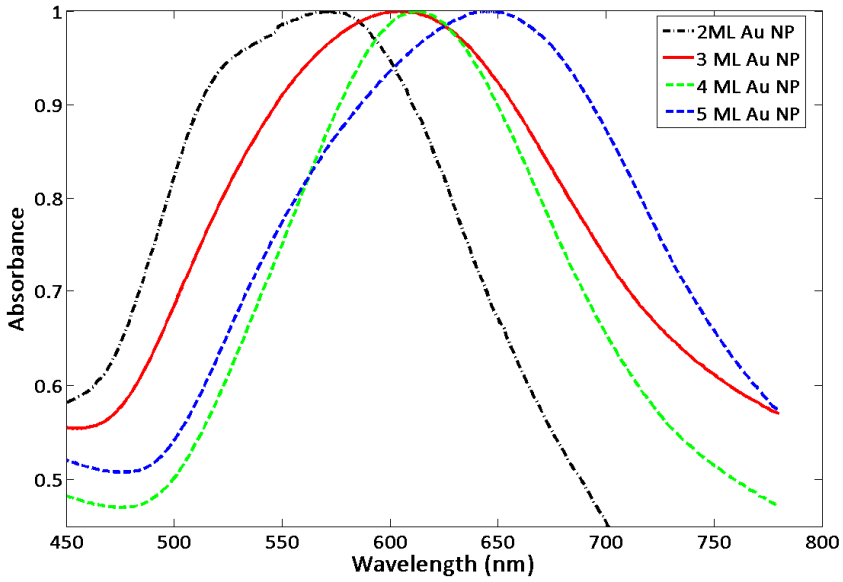

Figure 2. 2 Resonance frequency shift of our metal nanoparticle solids growing in size.

2.5 Emission Enhancement Using Localized Surface Plasmons

It is well known that emission of fluorescent molecules is effected by their environment as stated by Purcell in 1897. Thus it is not surprising that emission of molecules nearby metal nanoparticles is significantly altered relative to their absence [21]. Electromagnetic fields near metal nanoparticles can be significantly increased when the frequency of the incident field is in the regime of metal nanoparticles' resonance frequency. Then this amplification may in turn increase the emission process of nearby fluorescent molecules, but it is also possible that emission of fluorescent molecules in the close proximity of metal nanoparticles can be quenched through nonradiative channels of metal nanoparticles [22]. Thus, photoluminescence of fluorescent molecules near metal nanoparticles is altered

depending on the absorption, emission and dissipation rates in the nanoparticles complex.

Emission of a molecule depends on both excitation rate and the ratio of radiative emission to decay rate, which is defined as quantum yield of the molecule. This relation is given in (2.6).

$$\gamma_{em} = \gamma_{exc} \frac{\gamma_{rad}}{\gamma_{rad} + \gamma_{nrad}} \tag{2.6}$$

where γ_{exc} is the total recombination rate of the emitting molecule, and γ_{rad} and γ_{nrad} are radiative and nonradiative recombination rates.

Excitation rate is mostly influenced by incident field and the angle between the direction of the field and polarization direction of the molecule. Therefore, increasing the amplitude of incident field by means of localized surface plasmon resonance can increase the excitation rate. However, the quantum yield of the fluorescent molecule can be decreased as the nonradiative decay rate can be increased due to ohmic losses for being in close proximity to metal nanoparticles. The distance between the metal nanoparticles and emitting molecules is the most critical parameter as emission enhancement or quenching of the molecule can be controlled via varying this quantity. Generally, the decrease of quantum yield is greater than increase of excitation rate and overall emission is quenched for small distances as depicted in Figure 2.4. It is also mentionable to emphasize that ohmic losses increase dramatically at the resonance frequency of the metal nanoparticle. Hence excitation wavelengths that are red shifted relative to the resonance frequency results in better emission enhancement [23].

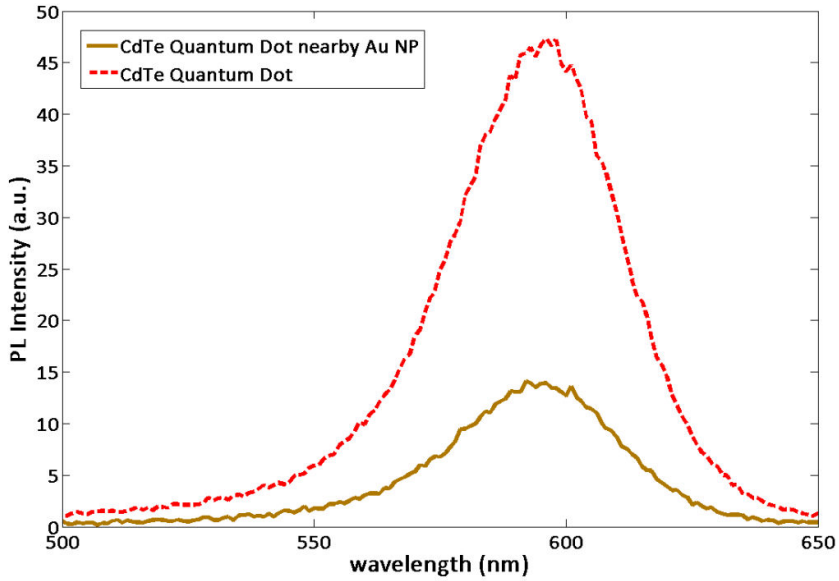

Figure 2. 3 Emission quenching of our CdTe quantum dots very close to metal nanoparticles.

As discussed above, to achieve enhanced emission of molecules in the proximity of metal nanoparticles there should be a certain separation between them. This condition can be satisfied, for example by sandwiching dielectric layers between metal nanoparticles and fluorescent molecules. However, if the thickness of these dielectric layers is too large, then there will not be strong plasmonic coupling between the particles. This situation is depicted in Figure 2.5.

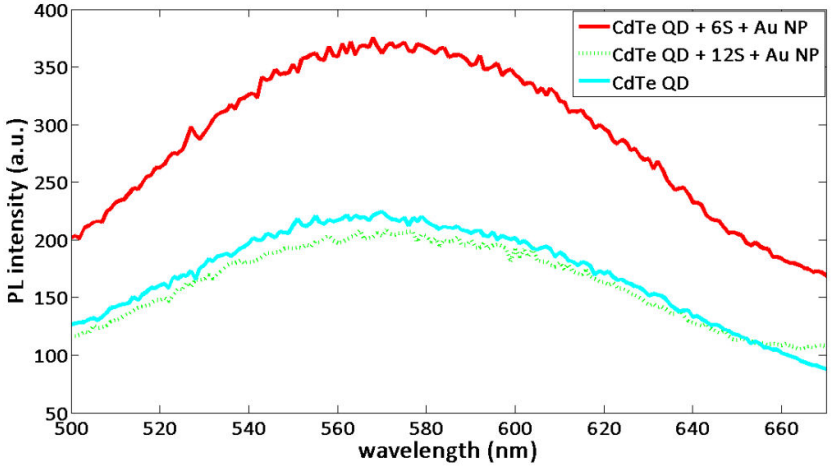

Figure 2. 4 Emission enhancement decreasing with increased thickness between our CdTe quantum dots and gold nanoparticles.

Size and orientation of fluorescent molecules are two other important factors apart from the distance between the molecules and the metal nanoparticles. Depending on these factors, exciton lifetime of the fluorescent molecules shortens as the energy transfer to the metal nanoparticles increases [24]. This energy transfer mechanism is nonradiative and similar to Förster resonance energy transfer that occurs between the acceptor and donor molecules. Strong coupling between excitons of fluorescent molecules and plasmons of metal nanoparticles may lead to more efficient and faster energy transfer.

Coulomb interaction is the main coupling mechanism since the distance between metal nanoparticles and fluorescent molecules is too small for treating the particles simply as dipoles while it is too far for carrier exchange to take place between the particles [25]. In this region, the exciton-plasmon coupling is strong relative to the case of large distances and exciton resonance is significantly increased as the field around the molecule is enhanced through plasmon coupling.

As illustrated in Figure 2.6(a), the distance between the metal nanoparticle and the semiconductor nanocrystal crystal is smaller than the radius of the metal nanoparticle and larger than the radius of the quantum dot. This distance is ideal

for strong exciton-plasmon coupling and emission enhancement. This system is excited by laser radiation which in turn stimulates both the transition dipole moment of fluorescent molecules and interband transitions of metal nanoparticles as it is depicted in Figure 2.6(b). The transition in metal nanoparticle couples to exciton in the molecule via Coulomb interaction. Thus, electric field inside the molecule is affected by laser radiation, plasmon induced field and plasmon-exciton interaction [26].

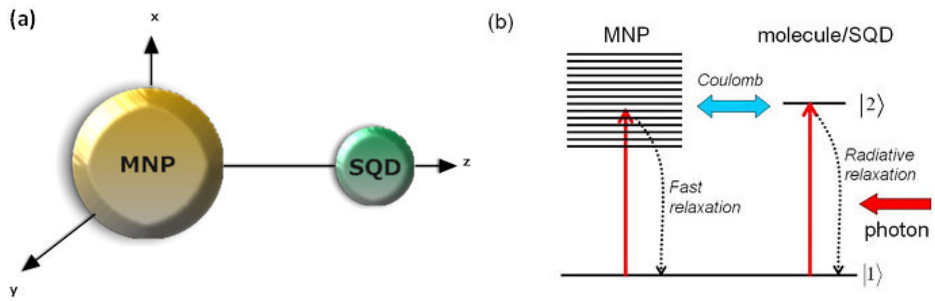

Figure 2. 5: (a) Dimensions of components and (b) coulomb interactions between a metal nanoparticle (MNP) and fluorescent molecule,e.g. semiconductor quantum dot [26].

Emission enhancement or quenching of quantum dot emitters can be better explained when the modification of radiative and non-radiative decay rates under the influence of plasmons is studied. Therefore, simple model of the basic system of Figure 2.6(a) is considered in an inductive manner by deriving equations (2.7-2.13).

In a metal-semiconductor nanoparticles complex, number of excitons in the semiconductor quantum dot is given by (2.7)

$$\frac{dn_{exc}}{dt} = -\gamma_{tot} n_{exc} + I_{abs} \tag{2.7}$$

where n_{exc} is the number of excitons and γ_{tot} is total recombination rate and I_{abs} is the absorption intensity inside the semiconductor.

Recombination rate of excitons in this complex is the result of three different rates, given by (2.8)

$$\gamma_{tot} = \gamma_{rad} + \gamma_{nrad} + y_{metal} \tag{2.8}$$

where γ_{rad} stands for the radiative recombination rate inside the semiconductor, γ_{nrad} is the nonradiative recombination rate and γ_{metal} is the nonradiative decay rate due to the nearby metal nanoparticle.

Both radiative recombination rate and absorption intensity of semiconductor nanocrystal is modified according to equations (2.9 and 2.10) when a metal nanoparticle is placed close to it.

$$I_{absm} = P(w_{exc})I_{abs} \tag{2.9}$$

$$\gamma_{radm} = P(w_{emis})\gamma_{rad} \tag{2.10}$$

where $P(w_{exc})$ and $P(w_{emis})$ are enhancement coefficients at excitation and emission frequencies respectively. Then, emission enhancement of semiconductor nanocrystals in the proximity of metal nanoparticles can be calculated by using equation (2.11).

$$E = \frac{P(w_{exc})P(w_{emis})\gamma_{tot}}{P(w_{emis})\gamma_{rad} + \gamma_{nrad} + \gamma_{metal}} \tag{2.11}$$

For semiconductor nanocrystals that have a quantum yield close to 1, we have equation (2.12) and for semiconductor nanocrystals that have a quantum yield close to zero we have equation (2.13).

$$E = \frac{P(w_{exc})P(w_{emis})\gamma_{tot}}{P(w_{emis})\gamma_{rad} + \gamma_{metal}} \tag{2.12}$$

$$E = P(w_{exc})P(w_{emis}) \tag{2.13}$$

Therefore, depending on the quantum yield of fluorescent molecule emission can be increased by either increasing radiative emission probability or absorption intensity.

2.6 Metal Nanoparticle Synthesis

To study plasmon coupling, we synthesized gold nanoparticles are synthesized using chemical reduction method. Materials used in this synthesis are chloroauric acid $HAuCl_4$ and trisodium citrate $Na_3C_6H_5O_7$ of analytical grade

purity that are purchased from Sigma Aldrich of UK. First, 20 mg of chloroauric acid is taken using a plastic spoon and at this point sunlight exposure of chloroauric acid should be prevented. Then, chloroauric acid is dissolved in 100 ml of Milli-Q water using a large stirrer in a beaker while 50 mg of trisodium citrate is taken and dissolved in 5 ml of Milli-Q water using a sonicator. The beaker of chloroauric acid dissolved in water is heated until it boils and trisodium citrate is also heated in a separate beaker for preventing sudden cooling of the reaction beaker. Then, trisodium citrate dissolved in Milli-Q water is poured into the reaction beaker as the solvent inside the beaker boils. As the reaction starts, the transparency of the solution increases. After a few minutes, color of the solution turns to black and this color slowly fades to red in time. At this point, the solution is left boiling for 15 minutes and at the end of 15 minutes it reaches its final red color that looks like red wine. Finally, the solution is cooled for an hour.

The size of the synthesized gold nanoparticles is approximately 20 nm with a 10% size distribution. We deposited them as layers of thin films using layer by layer deposition technique (as will be explained in chapter 3) and they effectively aggregate into larger solids depending on how many layers are deposited, which controls the resulting size of particles in the thin film. In Figure 2.7, atomic force microscop (AFM) graphs of 2 and 5 monolayers of thin film gold nanoparticles are given.

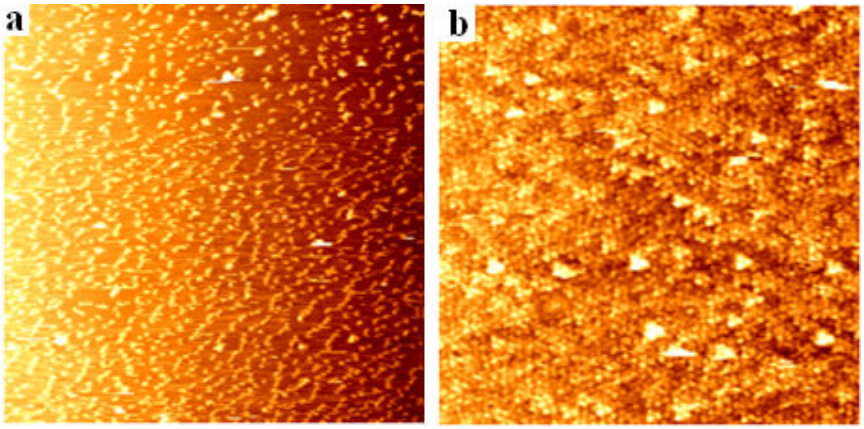

Figure 2. 6 AFM graph of our gold nanoparticles of 2 (a) and 5 (b) monolayers in thin film.

Chapter 3

Synthesis and Thin Film Deposition of Colloidal Quantum Dots

Characteristic length scales that affect many physical phenomena occurring in materials are mostly in the nanometer size regime [27]. Therefore, it is expected to experience new physical phenomena that are neither revealed in molecules nor bulk form of the materials when nanoscale materials are considered.

Especially, electronic and optical properties of semiconductor nanocrystals and metal nanoparticles depend on the size of the particles. Size of the semiconductor quantum dots(QD) range from 2 to 20 nm (Figure 3.1) and varying the size of quantum dots leads to modification of their bandgap. Unlike the bulk or molecular counterparts of the semiconductor materials, this variable bandgap of quantum dots allows for tailoring optical and electronic properties of materials. This unique property of quantum dots provides an easy access to a wide range of colors. Also, when they are compared with organic fluorophores, quantum dots are much brighter and they do not photobleach. Hence, they have attracted great interest over the past two decades and research has been carried out for both physical properties and technical applications of these nanoscale materials. Today, they still attract great attention as both their shape and composition can be tailored and they can be assembled into complex structures such as supercrystals. They can be utilized as biological tags and be fabricated into devices including solar cells, lasers and light emitting diodes.

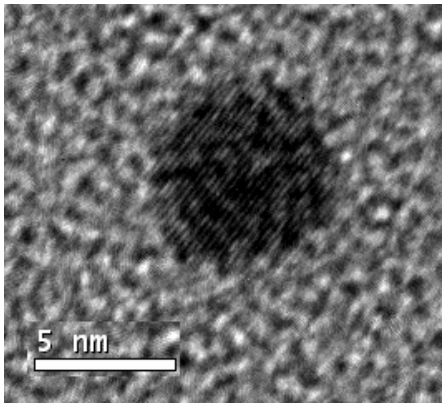

Figure 3. 1 Transmission electron microscope graph of a colloidal quantum dot synthesized at our nanomaterial synthesis laboratory.

3.1 Semiconductor Quantum Dots

Atoms have discrete energy states that are filled by electrons. However, as the atoms combine together to form materials, these discrete energy states forge into almost continuous energy bands such as valence and conduction bands.

Semiconductor materials have energy gaps between the valence and conduction energy bands and it is quantum mechanically forbidden for electrons to exist in this region. Photons that have energy close to the energy gap of the semiconductor or more can be absorbed and electron-hole pair (exciton) is created [28].

For bulk semiconductors, the width of the energy gap is solely determined by the composition of the material; hence, it does not change as the size of the material varies. However, size of the nanomaterial also affects the width of the energy gap and energy bands since natural length scales of electron, hole or electron-hole pair are close to the size of such quantum confined material [29]. This effect is known as the quantum size effect and these length scales can be calculated using (3.1),

$$a_B = \varepsilon \frac{m}{m^*} a_0 \tag{3.1}$$

where a_0 is the Bohr radius, ε is the dielectric constant of the medium and m and m* are the rest and effective masses of electron and the considered particle.

Depending on how small the material is either all of the particles (electron, hole or electron-hole pair) or some of them can be confined in the boundaries of the material. Thus, three different size regimes arise as strong, weak and intermediate confinement regimes and each one of them has different effects on the structure of electronic states such as changing the shape of the energy bands and discretizing them. Nanoscale materials that exhibit this behavior are named depending on the number of confinement dimensions as quantum wires (nanorods) and quantum dots (nanocrystals). Quantum dots correspond to three dimensional confinement of the material and the width of their bandgaps is characterized by their diameters, in addition to their composition (Figure 3.2).

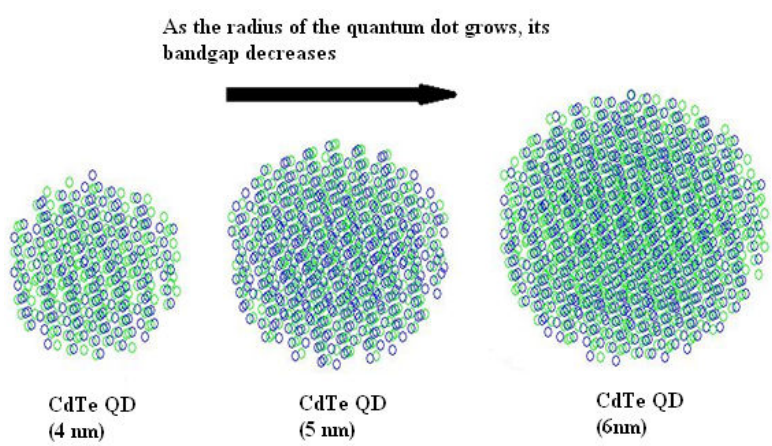

Figure 3. 2 Illustration of atom stacking CdTe quantum dots from our simulations.

As the diameter of the quantum dot decreases, strength of the quantum confinement grows stronger and the bandgap of the material increases while the continuous conduction and valence bands split into further discrete states. Even though the wavefunction of electrons and holes extends to thousands to millions of atoms, electrical response of quantum dots is discrete. Thus they can be

considered as quasi-atomic particles [30]. This physical phenomenon can be expressed by considering a quantum box and energy gap of the quantum dot is roughly given by (3.2):

$$E_g = E_{g0} + \frac{h^2}{4m_{eh}R^2} \tag{3.2}$$

where E_{g0} is the bandgap of the bulk semiconductor, m_{eh} is the effective electron hole mass, h is Planck's constant, and R is the radius of the quantum dot.
or absorption intensity.

3.2 Colloidal Quantum Dot Synthesis in Aqueous Medium

Colloidal quantum dots, also referred to as nanocrystals, are grown in solution and stabilized by a layer of surfactants via surficial attachment [31]. Prominent properties of these nanocrystals can be changed via varying size, shape and composition of core inorganic material, while stabilization, fabrication and assembly of these particles are provided by surfactants.

Colloidal nanocrystal synthesis mainly relies on the use of precursors, organic surfactants and solvents. Precursors are generally organic compounds of metals such as cadmium and common properties of precursors are fast decomposition and short reaction time. Also, the residuals of the reaction leave the medium easily.

Organic surfactants are chosen to be easily adhering molecules to nanocrystal surfaces since adhesion of surfactant is critical for determining size and shape during growth of nanocrystals. Another important property of organic surfactants is to provide dynamic solvation at the growth temperature as nanocrystals should keep growing by the addition of monomers for large sizes, while aggregation of nanocrystal cores is prevented. As the temperature decreases, these particles tend to stay in the surfaces of the nanocrystals and they

thus provide stability of the structure. Also, some parts of organic surfactants are responsible for solubility of the quantum dots, which determines solvents to be used.

Temperature controlled heating is important for colloidal nanocrystal synthesis. Final temperature is generally chosen in the range of 200 – 400 °C, at which both stability of organic material and melting of inorganic nanocrystals can be provided. Bulk form of CdTe melts at 1092 °C, whereas 300 °C is sufficient for nanoscale counterpart.

Colloidal nanocrystal synthesis begins with the addition of precursors and after precursors turn into chemically active monomers thorugh heating, chemical reaction is initiated and supersaturation of the medium leads to nucleation followed by the growth of nanocrystal nuclei with excess monomers.
Monomer concentration is very critical since size distribution of the syhthesized nanocrystals will eventually be set depending on this quantity. Low monomer concentration leads to broadening of size dispersion; however, low monomer concentration also enables slow growth rate due to Ostwald ripening and number of small nanocrystals shrink as they add to large nanocrystals.

Following the colloidal nanocrystal synthesis, several methods such as size selective precipitation are used for narrowing down the size distribution. It is also possible to achieve simultaneous growth of small nanocrystals by means of rapid injection. But slow growth rate is generally preferred for obtaining nearly spherical and large nanocrystals. At the end of colloidal synthesis, considerable amount of monomers are placed on the surface of NCs and an interface of inorganic-organic layer is formed.

Achieving monodispersive nanocrystals by means of size, shape, crystal structure and surficial property is necessary for studying physical properties of these particles. Most of the nanocrystals synthesized have size in the range of 2-

10 nm, where both mean value and standard deviation of size can be precisely predefined similar to the synthesis of polymers. Two decades of progress has been leading nanocrystal synthesis of well-defined structures. Methods used for synthesis include coprecipitation in aqueous phase, using reverse micelles as templates, solvothermal synthesis, hydrothermal synthesis and hot injection [32, 33].

We synthesize CdTe quantum dots in aqueous medium at our nanomaterial synthesis laboratory using hot injection method. Materials used in this synthesis are aluminum telluride (Al_2Te_3) and cadmium perchlorate hexahydrate ($Cd(ClO_4)_26H_2O$) as precursors, thioglycloic acid (TGA: $(SH)CH_2COOH$) as the organic surfactant, Milli-Q water, sodium hydroxide (NaOH), sulfuric acid (H_2SO_4) and iso-propanol (C_3H_7OH) as solvents and such.

In Step 1, 4.59 gram cadmium perchlorate hexahydrate and 250 ml Milli-Q water are mixed in a 1l round bottom 3-neck reaction flask and the mixture is stirred with a magnetic stirrer vigorously until all of the cadmium perchlorate hexahydrate is dissolved in water as the solution becomes transparent.

In Step 2, 250 ml Milli-Q water is added in small amounts into a small vial containing 1.33 gram thioglycloic acid. Then, the mixture is poured into the large flask containing cadmium perchlorate hexahydrate and 250 ml Milli-Q water solution. This step continues until no smell of thioglycloic acid is detected from the small vial. Finally, rest of the Milli-Q water is poured into the large flask.

In Step 3, pH value of reaction flask is adjusted by adding NaOH solution slowly since after some drops pH value grows dramatically. At the end, the pH value of the reaction flask should lie between 11.8 and 12.0.

In Step 4, 800 mg of aluminum telluride is taken into a 25 ml 3-neck flask in the glove box (Figure 3.2). All the necks of the flask are covered with either septa or parafilm in order to prevent aluminum telluride from oxidizing.

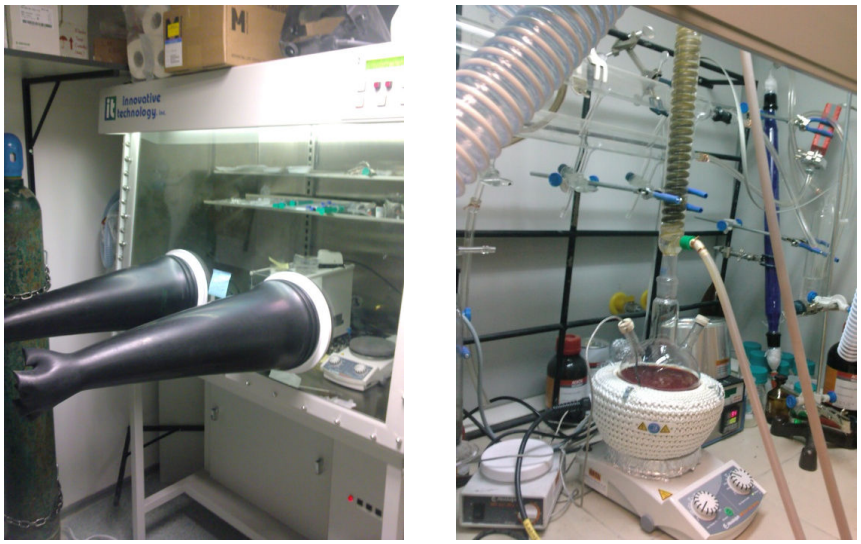

Figure 3. 3 Our glove box and experimental synthesis setup in the fume hood.

In Step 5, 0.5 molar H_2SO_4 solution is prepared for later use and the following setup is assembled. Argon is flowed through the system for approximately one hour to remove all the O_2 in the system.

In Step 6, H_2SO_4 is taken by a syringe and dropped into the small flask containing aluminum telluride through the septum closing the neck. As the reaction takes place, H_2Te gas is generated and carried to the large flask via argon flow in the system. After half an hour, small flask is separated from the large flask and the neck of large flask is closed again.

In Step 7, heating mantle is placed under the reaction flask and the flask is heated for boiling the mixture inside. At this boiling temperature, CdTe quantum dot growth begins. As the size of the quantum dots increases, their emission color shifts to longer wavelengths (Figure 3.3).

In the final step, either small aliquot can be taken for checking the growth of quantum dots as time passes or the reaction is stopped by cooling the system when the synthesized CdTe quantum dots reach the targeted diameters. Then, the solution is filtered to remove the remnants of the reaction. Finally, to obtain monodisperse quantum dots size selective precipitation methods are applied.

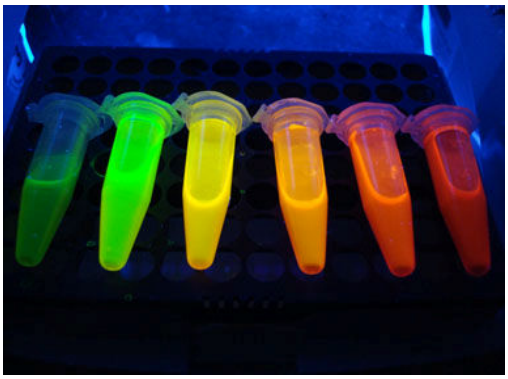

Figure 3. 4 Color variation of our CdTe quantum dots at our nanomaterial synthesis laboratory.

3.3 RF Characterization of Colloidal Quantum Dots

To measure QD dipole moments, we designed and fabricated a micrometer-scale on-chip measurement setup in parallel plate capacitor architecture. The two electrode plates, made of Ti/Au layers, were microfabricated on a Si substrate. The spacing between the plates was set to be 70 μm with a lateral housing of 1 cm^2 in cross-sectional area to place our QDs in solution. TOPO-capped QDs, as shown in Figure 1(a), were prepared using ligand exchange, for TOPO does not affect RF measurements. The external bias applied across the plates that house our TOPO-capped QDs in solution enforces alignment of QDs as sketched in Figure 3.5(a).

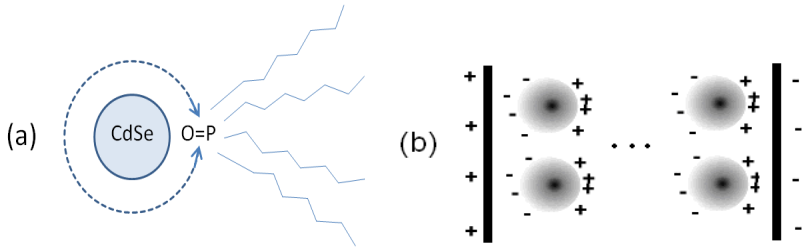

Figure 3. 5 (a) TOPO-capped CdSe QD (with only one TOPO ligand shown in the sketch for the sake of clarity) and (b) alignment of QDs when an external bias is applied across the plates of the microfabricated on-chip setup.

We implemented two different methods to measure dipole moment of our QDs. One of them relies on measuring capacitance as a function of operating frequency by an impedance analyzer (IA), whereas the other one is based on taking S-parameter spectral measurements by a programmable network analyzer (PNA). In both of these methods, the measurements were performed before and after the QDs were placed in the housing. As a result, we determined the relative dielectric constant dispersion by normalizing each measurement in the presence of QDs to that in the absence of QDs. Using several equations including Claussi-Mosotti equation we obtained the dipole moments of CdSe QDs in three different sizes and a pair of CdSe core and CdSe-ZnS core-shell QDs of similar size.

Figures 3.6, 3.7 and 3.8 represent the experimental data obtained using both IA and PNA. The results of these two independent measurements are in good agreement. Here we observed that *1.)* the dipole moments of these CdSe QDs are proportional to their sizes, *2.)* their dipole moments do not show dramatic changes over a wide range of operating frequency characterized in our experiments, and *3.)* core-shell structure shows greater dipole moment than only core structure of similar size. Currently, further experiments are underway to understand the increased dipole moment in core-shell structures as opposed to only core structures. Therefore, we measured the dipole moments of CdSe QDs synthesized in different sizes and structures by implementing two different RF measurement methods, one using impedance analyzer and the other using programmable network analyzer.

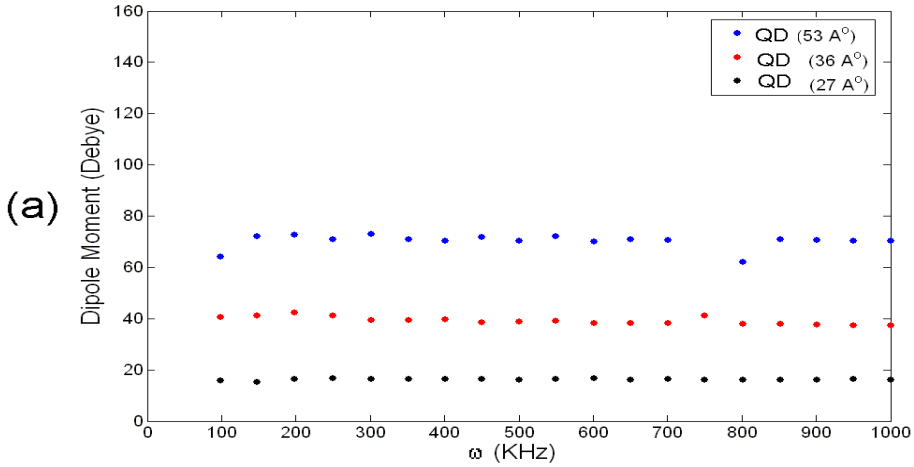

Figure 3. 6 Dipole moment of TOPO-capped CdSe QDs in different sizes (27 Å, 36 Å, and 53Å) measured as a function of operating frequency by impedance analyzer.

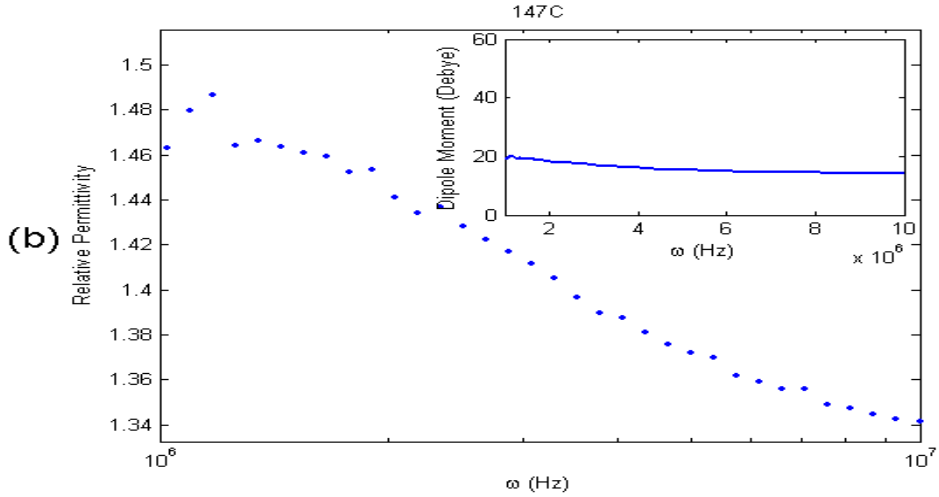

Figure 3. 7 Relative permittivity and dipole moment (in the inset) of TOPO-capped CdSe QD (27 Å) measured as a function of operating frequency by programmable network analyzer.

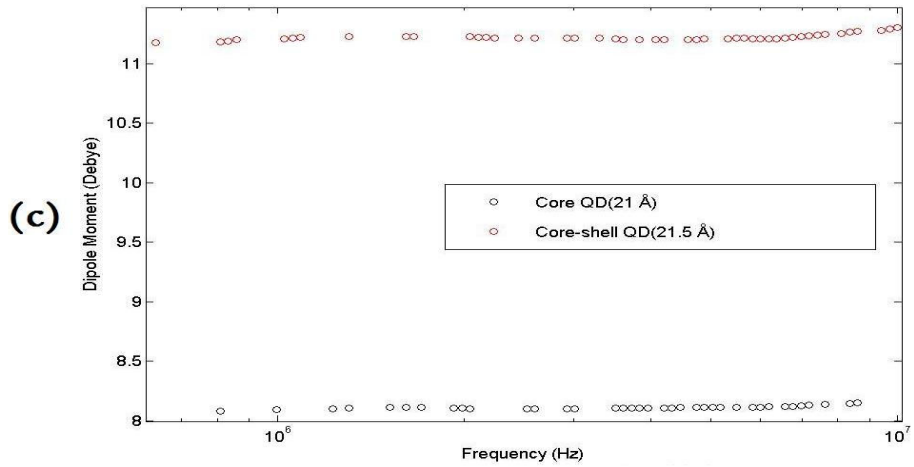

Figure 3. 8 Dipole moments of TOPO-capped CdSe core QD (21 Å) and CdSe-ZnS core-shell QD (21.5 Å) measured as a function of operating frequency by programmable network analyzer.

3.4 Optical Characterization of Colloidal Quantum Dots

We make the optical characterization of colloidal quantum dots in either solution or film using Cary UV-VIS spectrophotometer to record absorbance spectra and Cary Eclipse fluorescence spectrophotometer to take photoluminescence spectra. Absorbance spectra of our synthesized CdTe quantum dots of varying sizes are shown in Figure 3.9.

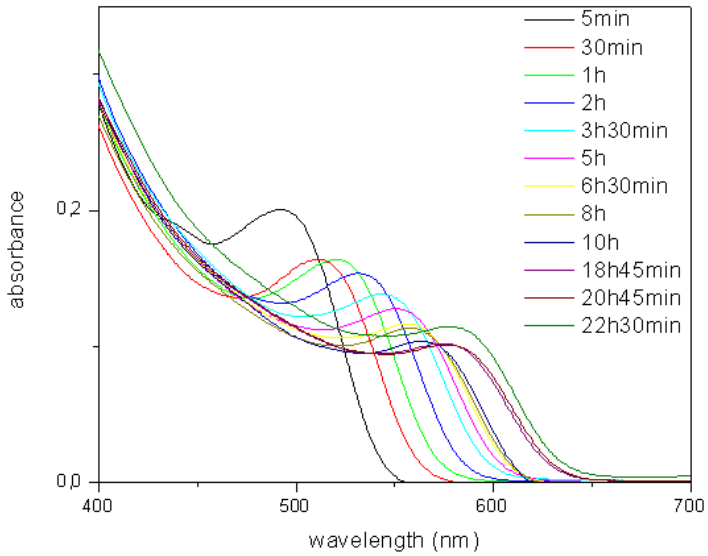

Figure 3. 9 Absorption spectra of our CdTe quantum dots of varying size controlled by reaction growth time (from 5 min. to 22 h. 30 min.).

As the absorbance spectra of CdTe quantum dots in Figure 3.9 illustrates the first exciton absorption peak of quantum dots shifts to longer wavelengths if their growth time increases. This observation is a natural result of the fact that the bandgap of quantum dots decreases as their size thereby grows and less energetic photons make optical transitions across their effective bandgap at longer wavelengths. It should be also noted that for further shift of the first exciton absorption peak much longer time of growth is necessary. This is inevitable because Oswald ripening, which enables the growth of quantum dots is a slow process even requiring several days [34].

The data obtained from these absorbance spectra can be used to find either extinction coefficient or concentration of quantum dots in solution by using Lambert-Beer's law if one of the two is known [35]. For thin films of quantum dots relative concentrations of particles can be obtained by calculating the areas under the absorbance spectra and rating them with respect to each other.

Photoluminescence spectra of our synthesized CdTe quantum dots are shown in Figure 3.10. As in photoluminescence is the case in the absorbance spectra of these quantum dots, the peak position of the curves in Figure 3.10 also shifts to longer wavelengths as the growth time increases. This observation can also be explained with the same reasoning.

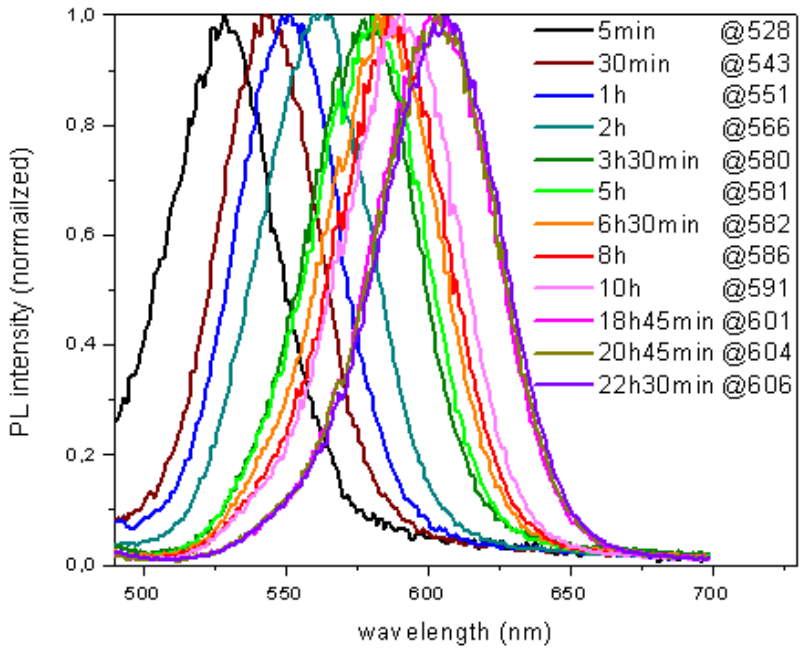

Figure 3. 10 Photoluminescence spectra of our CdTe quantum dots of varying size controlled by growth time (from 5 min. to 22 h. 30 min.).

Exciton lifetime measurements are conducted using our time-resolved fluorescence setup (picoquant). Photoluminescence decay curves of CdTe quantum dots emitting in green and red are compared in Figure 3.11. As can be seen from the figure, green emitting CdTe (560 nm) quantum dots have shorter exciton lifetimes than red emitting CdTe (640 nm) quantum dots. This observation is expected since quantum dots with larger bandgaps (or larger transition dipole moments) decay faster [36]. Also, quantum dot photoluminescence intensities at peak wavelengths can be compared by using this setup in constant time mode.

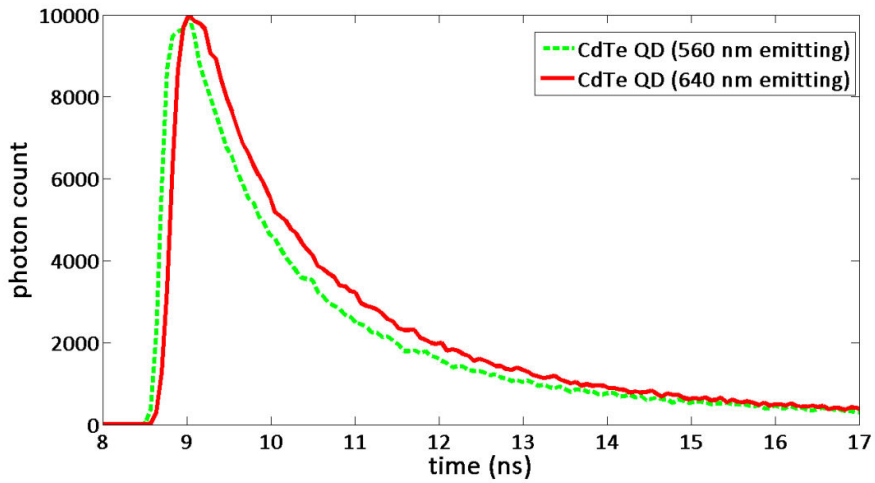

Figure 3. 11 Time-resolved fluorescence spectra of our CdTe quantum dots with two different sizes (emitting at 560 and 640 nm peak wavelengths).

3.5 Colloidal Quantum Dot Thin Film Deposition

Nonradiative energy transfer mechanism mainly depends on the distance between the interacting molecules. Therefore, fabrication techniques that enable controlled separation between different types of molecules are extremely important. Several methods including Langmuir-Blodgett and self-assembly are used to fabricate monolayer and multilayer films over the past few decades [37]. Layer by layer deposition technique is developed at early nineties and offers a simpler assembly approach for developing multilayer films relatively less dependent of the substrate size and topology on which they grow [38]. This method utilizes electrostatic attraction forces between oppositely charged layers hence positively and negatively capped layers are deposited one after another in the desired construction. In Figure 3.12, subsequent deposition of pairs of positively and negatively charged polymers and positively charged polymer and negatively charged nanoparticles starting over negatively charge glass substrate is depicted.

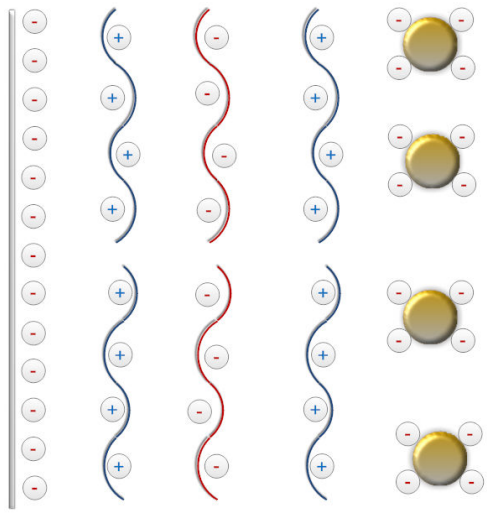

Figure 3. 12 Deposition of positively and negatively charged layers using layer by layer deposition technique.

Layer by layer deposition method starts with the deposition of a positively charged polymer layer on top of a substrate whose surface is negatively charged and is followed by a washing step for cleaning the sample from excessive polymer that is not properly adhered via Coulomb attraction. Next step is the deposition of negatively charged polymers or particles followed by a washing step again. In this cyclic manner, deposition of tens of layers is possible. The process flow of layer by layer deposition technique is illustrated in the Figure 3.13.

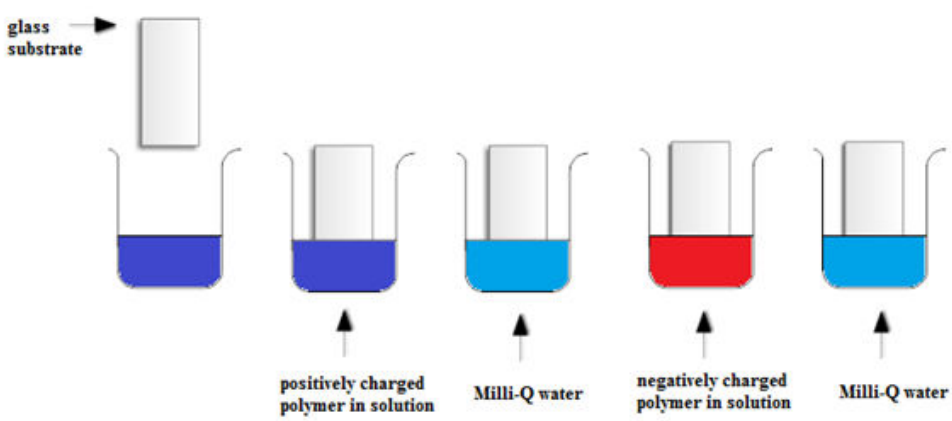

Figure 3. 13 Steps of layer by layer deposition method.

We use this deposition technique for fabricating multilayer films of quantum dots and metal nanoparticles with precisely controlled nanoscale spacing between them. First, surface treatment of glass slides that have nanoscale roughness on their surfaces is carried out by vibrating them in sonicator for approximately ten minutes in solutions of sodium hydroxide (NaOH), methanol (CH_3OH), acetone ($(CH_3)_2CO$) and iso-propanol(C_3H_7OH) in turn. By doing so, surfaces of the glass slides are negatively charged [39]. We use polydiallyldimethylammonium chloride (PDDA) as polyanion and sodium4-styrenesulfonate (PSS) as polycation to form polyelectrolyte bilayers. Both PDDA of 300 µl and 30 grams of PSS are dissolved in Milli-Q water that has 0.1M salt (NaCl) initially dissolved in it. Salt is used in these solutions because it provides swelling and breaks excessive bounds between PDDA and PSS and more homogeneous thin films are obtained [40]. Also, CdTe quantum dots are solved in salted Milli-Q water. Subsequently, repeated deposition of desired layers is conducted by a computerized dip coating system (manufactured by Nima Technology, UK) in a process program set with critical parameters including durations and speeds of immersing, withdrawing and holding in solution, which are optimized iteratively for our purposes.

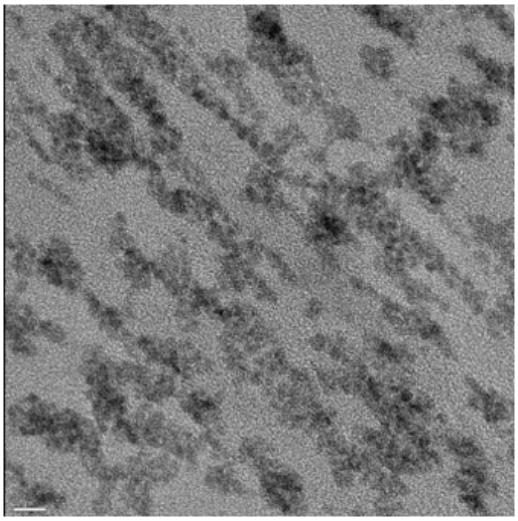

Figure 3. 14 Scanning electron microscop graph of our thin film CdTe quantum dot solids deposited by layer-by-layer assembly technique.

Chapter 4

Plasmon Mediated Nonradiative Energy Transfer

Förster type nonradiative energy transfer (FRET) is a well known physical phenomenon that takes place between donor and acceptor molecules in close proximity. Several parameters such as spectral overlap of emission spectrum of the donor molecule and absorption spectrum of the acceptor molecule, refractive index of the surrounding medium, relative orientation of transition dipole moments of the donor-acceptor pair and quantum yield of the donor molecule affect the rate and efficiency of the energy transfer between the donor-acceptor pair.

It is also well known that bandgaps of quantum dots can be tuned as explained in chapter 3 and two different sized quantum dots can be paired as donor and acceptor particles as one's absorption and other's emission spectrum can be matched. This allows for spectral control. Since thin films of quantum dot solids can be conveniently fabricated using a nanoscale deposition technique of layer by layer assembly as described in chapter 3, donor to acceptor distance, which is the most critical parameter in FRET, can be spatially controlled.

Plasmon coupled energy transfer is also non-radiative and can be achieved, e.g. via gathering a quantum dot and a metal nanoparticle in close proximity. Apart from relative distance between the quantum dot and the metal nanoparticle, a spectral overlap between emission spectrum of quantum dot and absorption spectrum of metal nanoparticle is critical for efficient energy transfer between them. To this end, both the emission spectrum of quantum dots and absorption

spectrum of metal nanoparticles can easily be adjusted by controlling their sizes. Also, thin films of metal nanoparticles can be fabricated using layer by layer assembly technique as the metal nanoparticles are synthesized to be negatively charged.

Since layer by layer assembly technique allows for the fabrication of thin films of tens of layers, thin films including metal nanoparticles, donor quantum dots and acceptor quantum dots with precisely controlled spacings in separate layers. Therefore, it is interesting and feasible to study strong plasmon-exciton coupling in a spatially and spectrally controlled way.

In this thesis, we study two different cases of strong plasmon-exciton coupling with 1.) plasmon coupling to only donor quantum dots and 2.) plasmon coupling to only acceptor quantum dots, while facilitating strong FRET between the donor-acceptor quantum dots at the same time.

4.1 Previous Literature and Contribution of This Work

Nonradiative energy transfer mechanism finds important applications in nanophotonics and nanobiology including nanoscale optical waveguiding and biological nanosensors [40, 42]. Various fluorophores can take part in such energy transfer interactions and their emission kinetics can thus be strongly modified. For example, colloidal semiconductor quantum dots, also known as nanocrystals (NCs), have widely been shown to serve as donors and acceptors among themselves or with other fluorescent species to transfer excitation energy nonradiatively in close proximity when the spectral conditions are set right. Emission characteristics of such fluorophores can be altered also when coupled with plasmonic structures, e.g., metal nanoparticles (MNPs), in their close proximity via strong plasmon-exciton interactions. One favored result of this plasmonic coupling mechanism is the spontaneous emission enhancement of

NCs. Recently plasmon-mediated Förster-type resonance energy transfer (FRET) has been demonstrated and FRET rate has been reported to be increased between acceptor-donor pairs of different species (including NCs) that are both plasmon-coupled [43, 16, 44]. In these previous reports, however, either donors and acceptors are blended and these blends are plasmon-coupled, or metal layer is placed between the donor and acceptor thin films to plasmon-couple both at the same time. In all of these prior works, the resulting plasmon-exciton interactions are not controlled to take place either at the donor site or the acceptor site but at both of the sites. Therefore it has not been possible to identify the coupled interactions. Here we present the first proposition and demonstration of cascaded plasmonic and nonradiative energy transfer interactions that are controlled by selectively plasmon-coupling either only donor NCs or only acceptor NCs of the energy transfer pairs. This scheme uniquely allows for the ability to spatially control plasmon-exciton interactions to take place either at the "start" site (donors) or "finish" site (acceptors) of the energy transfer. This control is achieved by placing the plasmonic layer in the right proximity of the donors (for strong donor-exciton plasmon-coupling) while sufficiently being far away from the acceptors (for weak acceptor-exciton plasmon-coupling), or vice versa. Here we comparatively study and analyze consequent modifications of NC emission kinetics in response to both cases of plasmon-coupling to only the donor NCs and to only the acceptor NCs through steady-state and time-resolved photoluminescence measurements, along with their lifetime and rate calculations.

4.2 Previous Literature and Contribution of This Work

Using the nanocrystal synthesis recipe described in Chapter 3, we synthesized CdTe quantum dots with emission peak wavelengths at 560 nm and 640 nm chosen as the donor and acceptor particles, respectively. We deposited thin films of these nanocrystals starting with 6 monolayers (MLs) of polyelectrolyte (PE)

bilayers followed by coating of 1 ML of quantum dot and finally covered by 1 ML of PDDA for improving film stability. Photoluminescence (PL) measurement of these thin films are conducted using Cary Eclipse spectrophotometer and absorbance measurement of the acceptor particle is conducted using Cary UV-Vis spectrophotometer. Spectral overlap of the absorbance spectrum of the acceptor nanocrystals and the emission spectrum of donor nanocrystals can be seen in Figure 4.1.

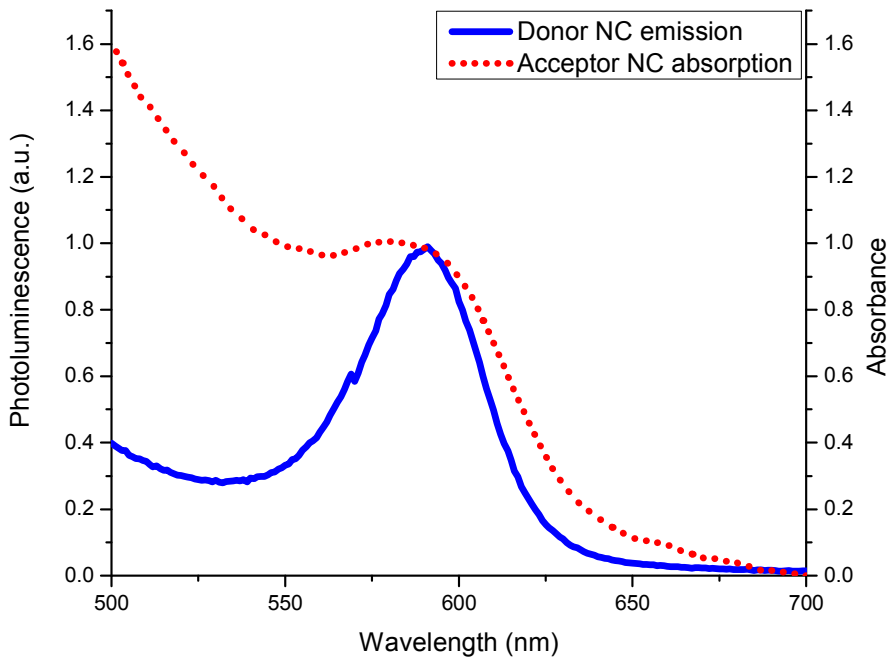

Figure 4. 1 Absorbance spectrum of our acceptor quantum dots and emission spectrum of donor quantum dots.

Fabrication of FRET sample is started with the deposition of 1 ML of PE bilayer (composed of PDDA and PSS) since quantum dot deposition is better achieved on top of a dielectric polymer layer instead of glass. Afterwards, 1 ML of donor quantum dots is deposited on top of PDDA layer and 3 ML's of PE bilayer are subsequently deposited to provide approximately 5 nm distance between the donor and acceptor MLs. Then, following 1 ML deposition of PDDA layer, 1 ML of acceptor quantum dots is deposited. Finally, 1 ML PDDA covers the top

of the structure. Layered architecture of this hybrid thin film is depicted in Figure 4.2.

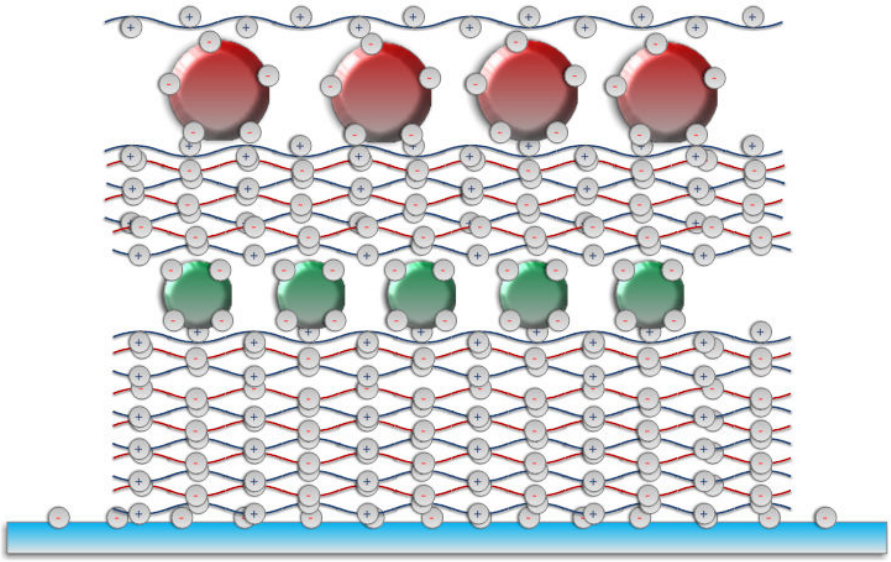

Figure 4. 2 Schematic representing the layered architecture of our FRET sample.

As expected, the emission of donor quantum dots is quenched in the presence of acceptor quantum dots while the emission of the latter dots is increased by 1.43 times because of nonradiative energy transfer from donor dots. Exciton lifetime measurements are conducted via time resolved fluorescence system and exciton lifetime of the donor quantum dots which is the critical parameter in determining energy transfer rate, is found to be shortened from 1.33 to 0.87 ns whereas the exciton lifetime of the acceptor nanocrystals is increased from 1.53 to 3.11 ns. Nonradiative energy transfer efficiency and rate are calculated using the exciton lifetimes of donor nanocrystals and found to be 0.35 and 0.39 ns^{-1} , respectively.

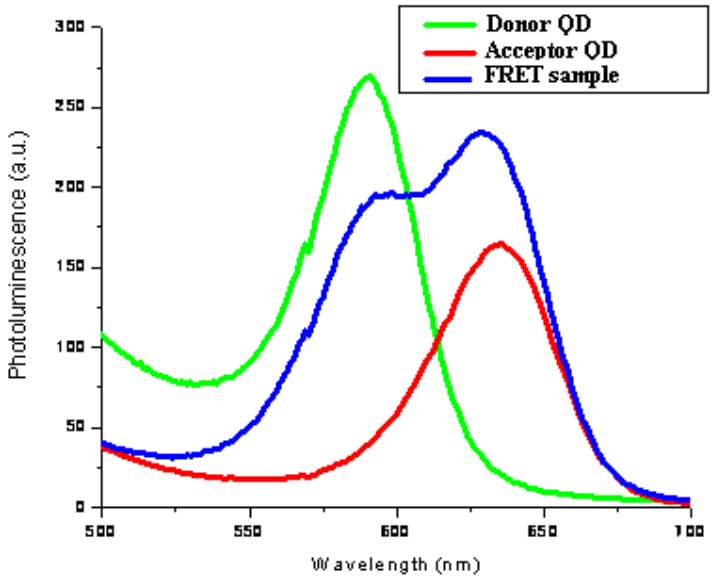

Figure 4. 3 PL spectra of our donor, acceptor and FRET samples.

4.3 Nonradiative Energy Transfer Using Plasmon Exciton Coupling

Energy transfer between semiconductor quantum dots and metal nanoparticles is possible in their close proximity when the spectral overlap between the emission spectrum of the quantum dots and absorbance of the metal nanoparticles is sufficiently large. When these conditions are satisfied, emission energy of the quantum dots is increased since the electric field inside and around the quantum dot is enhanced by the metal nanoparticle.

Since we chose CdTe quantum dots of emission peaks at 560 and 640 nm as the donor-acceptor pair, in order to satisfy strong plasmon-exciton interaction we deposited thin films of gold nanoparticles (Au NPs) that have plasmonic resonance wavelength centered close to 560 and 640 nm. To make the plasmon sample, deposition procedure starts with successive coatings of 1 ML PDDA and 1 ML gold nanoparticle for 3 or 6 monolayers that resulted in resonance

wavelengths of 560 and 640 nm, respectively. Then, 6 MLs of PE bilayer are deposited to achieve the desired distance between quantum dot layer and metal nanoparticle layers. Finally, 1 ML of donor or acceptor quantum dot layer is coated followed by deposition of 1 ML PDDA.

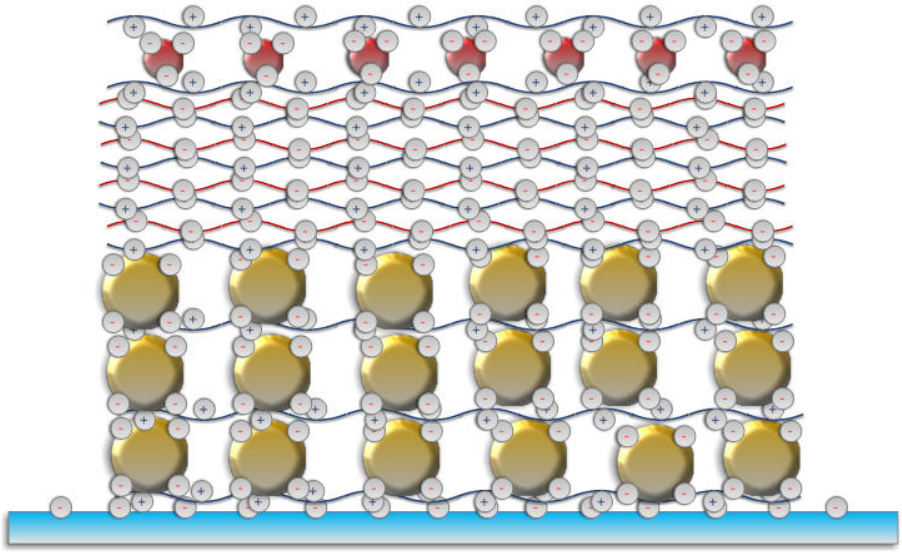

Figure 4. 4 Schematic representing the layered architecture of our plasmon sample.

Optical steady-state characterization of the prepared samples is carried out using the previously mentioned spectrophotometers (Figure 4.5). Emission of the acceptor nanocrystals is enhanced by a factor of 2.81 while emission of the donor nanocrystals is enhanced by a factor of 2.23 in the presence of metal nanoparticles. Exciton lifetime measurements of these samples are conducted using time resolved fluorescence (TRF) system (Figure 4.6 and 4.7). At the acceptor NC emission wavelength, in the presence of Au NPs coupled to acceptor NCs, the acceptor photon decay lifetime decreases from 1.53 ns to 0.97 ns (Figure 4.6). In the presence of Au NPs, donor NCs lifetime decreases down to 0.43 ns due to plasmon resonance energy transfer (Figure 4.7).

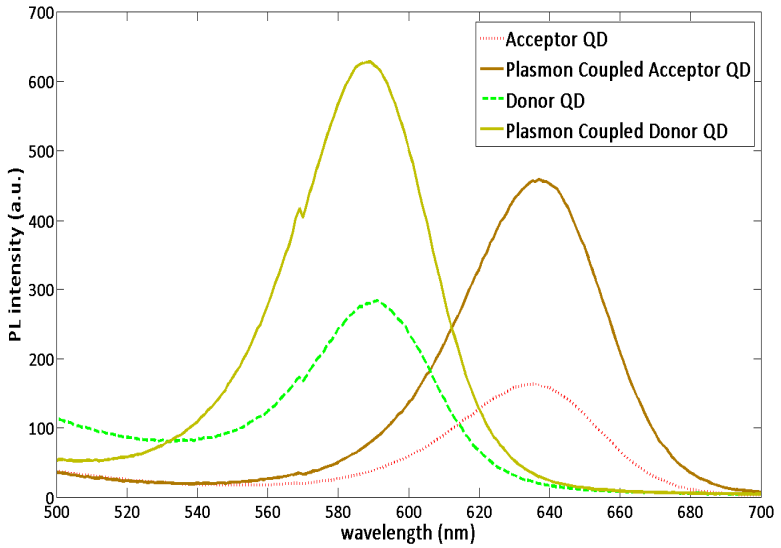

Figure 4. 5 PL spectra of our donor, acceptor, plasmon coupled donor, and plasmon coupled acceptor samples.

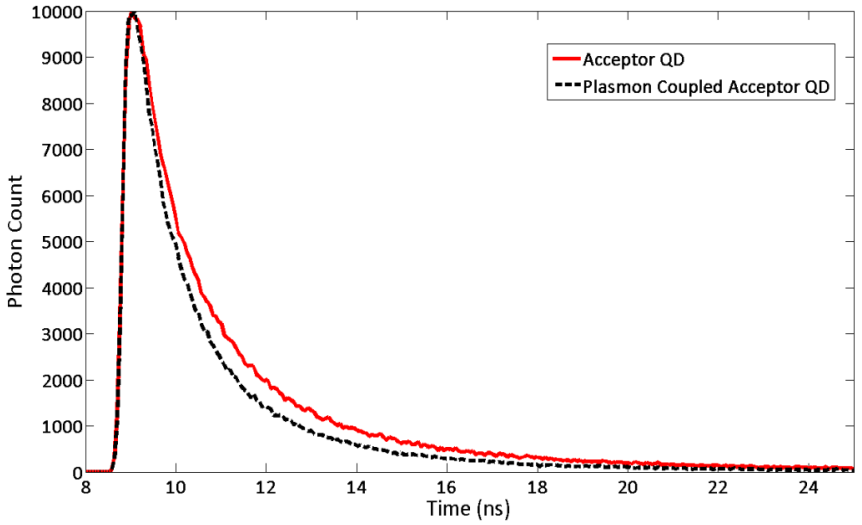

Figure 4. 6 TRF spectra of our acceptor and plasmon coupled acceptor samples.

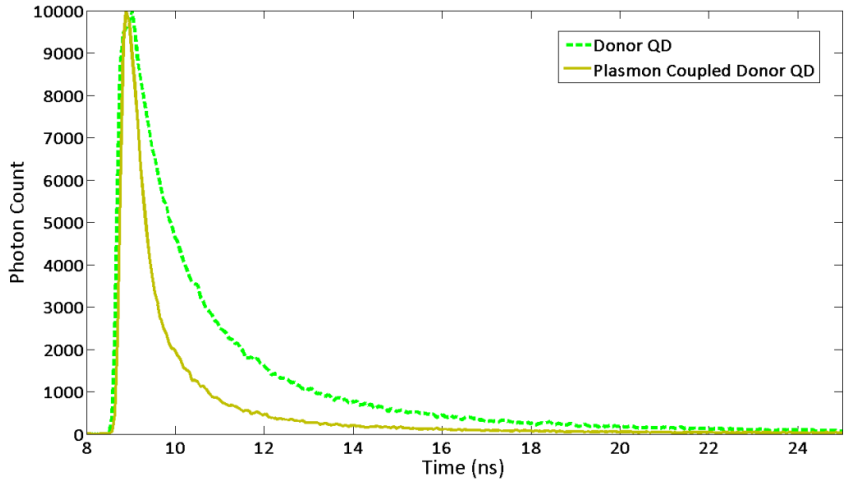

Figure 4. 7 TRF spectra of our donor and plasmon coupled donor samples.

4.4 Plasmon Mediated Nonradiative Energy Transfer between Quantum Dots and Metal Nanoparticles

In the previous two parts of this chapter, Förster type energy transfer and plasmon coupled energy transfer mechanisms are separately analyzed in terms of energy transfer efficiency, photoluminescence enhancement and energy transfer rate. In both of these energy transfer mechanisms, lifetime of the donor quantum dots that transfer their excitation energy is shortened and emission of at least one quantum dot is enhanced either via direct energy transfer in the case of FRET or via electric field enhancement in the case of plasmon coupling.

In the past few years, researchers have focused on studying the mechanism of the emission enhancement and quenching of a single semiconductor nanocrystal on the rough metal surface by changing incident light polarization and nanocrystal size [40]. They have also investigated the exciton coherent dynamics in the complexes composed of semiconductor quantum dots and rodlike metal nanoparticles [41]. They have presented experimental evidence for the enhanced FRET between CdTe quantum dots in nanoscale proximity to Au

NPs as well [42]. They have also demonstrated that the emission efficiency of type II QDs can be greatly enhanced by combining the FRET process with SPR [43].

In this part, plasmon mediated energy transfer, which is a far more complicated process relative to individual ones, is discussed in terms of energy transfer efficiency, photoluminescence enhancement and energy transfer rate. We analyzed our two proposed architectures by controlling the organization and inter particle distance such that plasmons of metal nanoparticles are either coupled to the acceptor nanocrystals or the donor nanocrystals, but not both unlike the previous studies.

4.4.1 Plasmon Coupling between Acceptor Quantum Dots and Metal Nanoparticles

As mentioned at the beginning of this chapter, in principle plasmons of metal nanoparticles can either couple to excitons of acceptor or donor nanocrystals of a FRET pair via tuning the sizes and the separation of the metal nanoparticles. In this part of the thesis, our aim is to analyze the architecture that favors strong plasmon coupling to the acceptor nanocrystals only, without any plasmonic interaction between the donor nanocrystals and the metal nanoparticles. Typical full-width at half maximum (FWHM) of the absorbance spectrum of the metal nanoparticles can be large enough to cover the emission peak of both the donor and acceptor nanocrystals. Therefore, instead of spectral control, selective plasmon coupling to the acceptors is achieved via spatial control. As a result, in this case, the distance between the donor nanocrystals and metal nanoparticles should be far enough to prevent coupling between them.

The deposition of this sample starts with 6 MLs of metal nanoparticle and positive polymer coating over glass slide. 6 MLs of PE bilayer are deposited in for the appropriate spacing between metal nanoparticles and nanocrystals to be coupled by plasmons. Afterwards, 1 ML CdTe nanocrystals emitting at 640 nm

(acceptors) and positive polymer are deposited. Subsequently, 3 MLs of PE bilayer are laid down for providing a controlled distance between the nanocrystal layers. Finally, 1 ML CdTe nanocrystal emitting at 560 nm (donors) and 1 ML of positive polymer are deposited. The architecture of our sample is sketched in Figure 4.8.

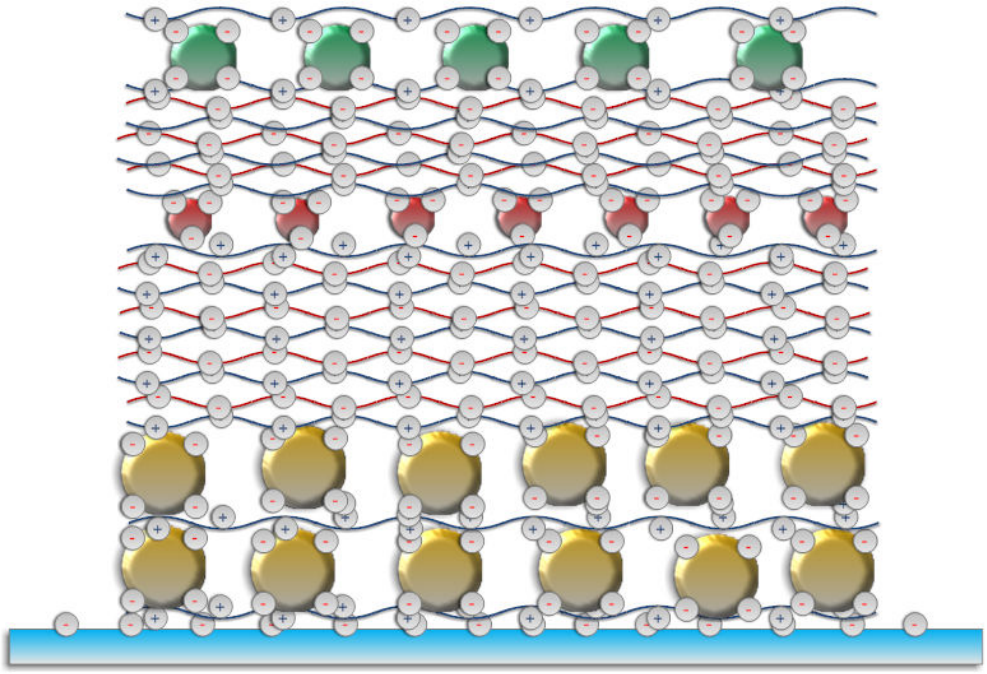

Figure 4. 8 Schematic representing the layered architecture of our plasmon coupled acceptor FRET sample.

As seen in Figure 4.9, emission of the acceptor nanocrystals that are both plasmon coupled (due to the presence of Au nanoparticles) and exciton coupled (due to the presence of donor nanocrystals) is increased with respect to the cases of both only nanocrystals and plasmon coupled nanocrystals. Here the emission enhancement of the acceptor nanocrystals is calculated to be 2.86 times the case of nanocrystals alone. This emission enhancement is the result of two different energy transfer mechanisms; the first one is the transferred energy from the donor nanocrystals and the second is the enhanced energy due to plasmon coupling.

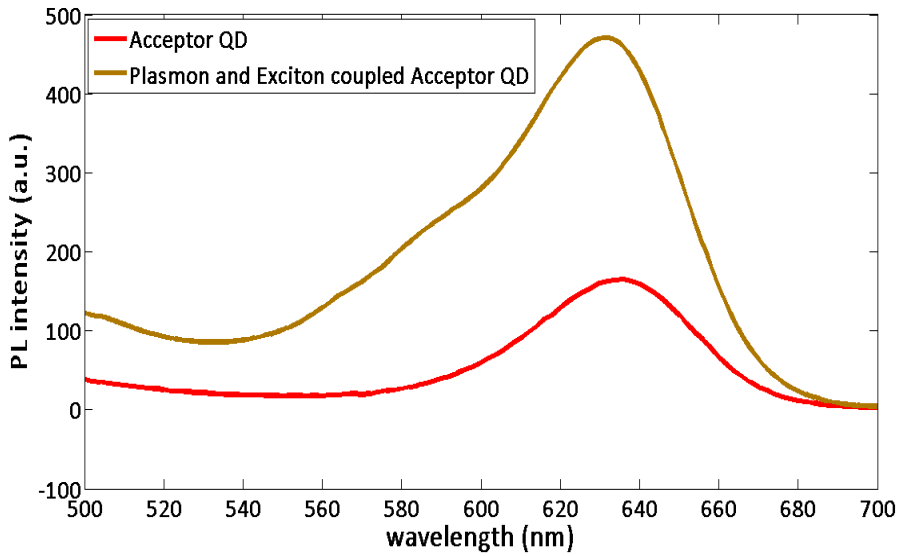

Figure 4. 9 PL spectra of our acceptor only sample and plasmon coupled acceptor FRET sample.

Exciton lifetime measurements of several samples are presented in Figure 4.10 and Figure 4.11. In Figure 4.10, the photoluminescence decay curves of donor nanocrystals are given for four different cases. The lifetime of the donor nanocrystals is not altered, when 12 monolayers of dielectric polyelectrolyte spacer is coated between them and the gold nanoparticles, and is found to be 1.31 ns, which is very close to its initial value in the absence of gold nanoparticles. Thus, we can definitely conclude that there is no plasmon coupling between the gold nanoparticles and the donor nanocrystals so the energy transfer from the donors is only to the acceptor nanocrystals in our complex sample. In this sample where the gold nanoparticles are coupled to the acceptor nanocrystals, the decay lifetime of the donor nanocrystals is found to be 0.89 ns which is very close to its value in the FRET sample. This also proves that there is no interaction between gold nanoparticles and donor nanocrystals.

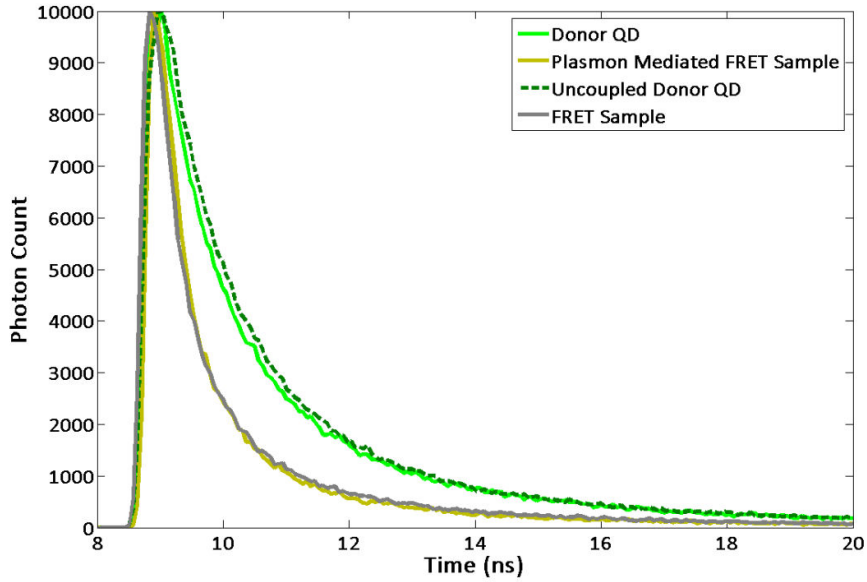

Figure 4. 10 TRF spectra of our donor, FRET, uncoupled donor and plasmon mediated FRET samples.

In Figure 4.11, the decay lifetime of the acceptor nanocrystals is presented in the presence of both gold nanoparticles and donor nanocrystals. Since the gold nanoparticles are coupled to the acceptor nanocrystals, a reduction in the lifetime of the acceptor nanocrystals is expected. However, because of FRET between the donor and acceptor nanocrystals, the lifetime of the acceptor nanocrystals should be increased. The decay lifetime of the acceptor nanocrystals is measured to be increased from 1.52 ns to 1.91 ns, which is smaller than the case in the FRET sample (in the absence of gold nanoparticles.) So, we can conclude that coupling between the donor and acceptor nanocrystals is strong even in the presence of gold nanoparticles.

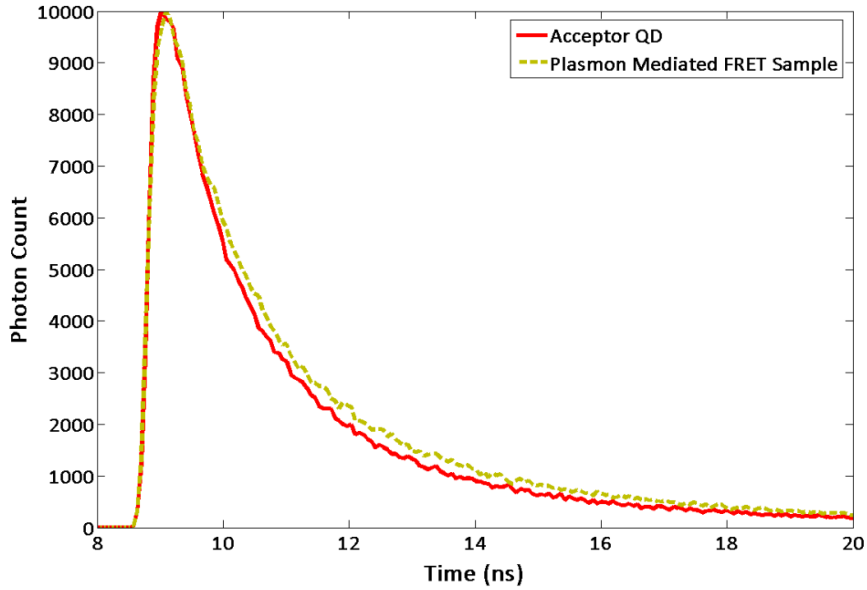

Figure 4. 11 TRF spectra of our acceptor and plasmon mediated FRET samples.

4.4.2 Plasmon Coupling Between Donor Quantum Dots and Metal Nanoparticles

In this section, plasmons of the metal nanoparticles are coupled to the donor nanocrystals, for which the absorption spectrum of MNPs and the emission spectrum of donor nanocrystals strongly overlaps. Since the peak of the emission spectrum of the acceptor nanocrystals are 80 nm far away from the donor nanocrystals, the spectral overlap between the emission spectrum of the acceptor nanocrystals and the absorption spectrum of the metal nanoparticles is weak. Furthermore, the acceptor nanocrystals are deposited far away from the metal nanoparticles as several dielectric layers are deposited in between.

The deposition of this sample starts with 3 MLs of metal nanoparticle and positive polymer coating over glass slide. 6 MLs of PE bilayer are then deposited to provide appropriate distance between the metal nanoparticles and the nanocrystals to be coupled by plasmons. Afterwards, 1 ML CdTe nanocrystals emitting 560 nm (donors) and positive polymer are deposited.

Then, 3 MLs of PE bilayer are deposited to obtain a controlled distance between the nanocrystal layers. Finally, 1 ML CdTe nanocrystals emitting at 640 nm and 1 ML of positive polymer are deposited. The architecture of this sample is depicted in Figure 4.12.

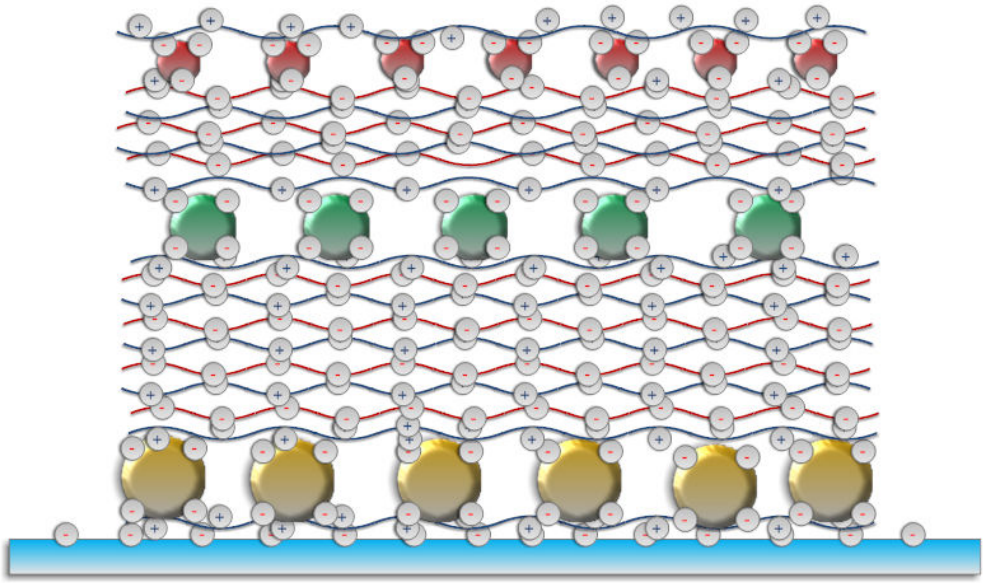

Figure 4. 12 Schematic representing the layered architecture of our plasmon coupled donor FRET sample.

Figure 4.13 shows the photoluminescence spectra of only donor NC, only acceptor NC, plasmon coupled donor NC samples and plasmon mediated FRET sample for donor plasmon coupled case. Emissions of both donor and acceptor nanocrystals are enhanced to the cases of individual nanocrystal. Also, emission of donor NCs is increased, but is yet weaker compared to only plasmon coupled sample. This reduction is also expected since some part of the energy is transferred from donor NCs to acceptor NCs due to FRET. Here the emission of acceptor NCs is increased by 2.26 times which is larger than the case of FRET sample.

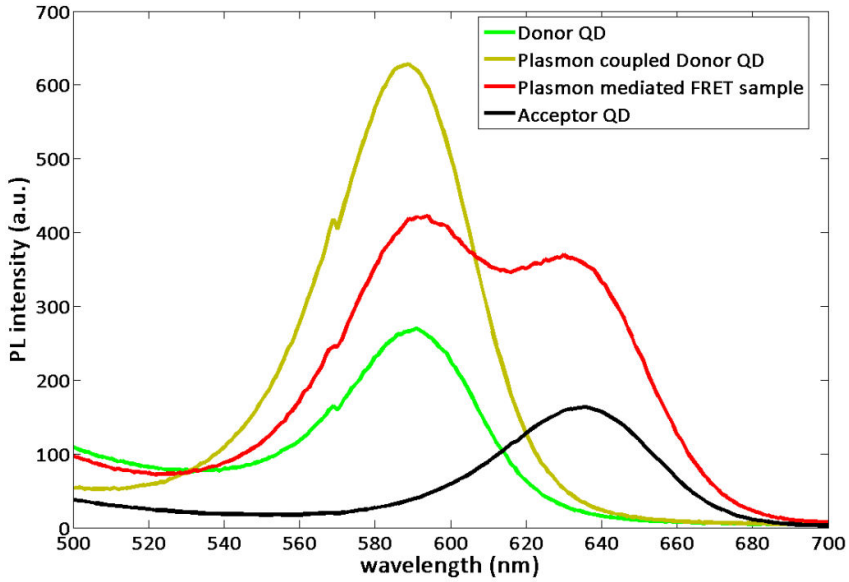

Figure 4. 13 PL spectra of our donor and plasmon coupled donor FRET samples.

Exciton lifetime measurements of these samples are given in Figure 4.14 and Figure 4.15. Figure 4.14 shows the decay lifetimes of the acceptor nanocrystals for four different cases: in individual nanocrystal sample, in uncoupled sample where 12 monolayers of dielectric layer is deposited in between acceptor NCs and gold nanoparticles, in FRET sample and finally in plasmon mediated FRET sample. As expected, exciton lifetime of the acceptor nanocrystals is not significantly changed for the individual nanocrystal and uncoupled samples and measured to be 1.44 ns instead of 1.51 ns. This shows the desired situation of uncoupling between the gold nanoparticles and the acceptor nanocrystals. In FRET sample, lifetime of the acceptor nanocrystals is increased to 3.11 ns and, in the plasmon mediated FRET sample it is increased from 1.51 to 3.91 ns. Both of these samples show the strong coupling between the acceptor and donor nanocrystals due to FRET.

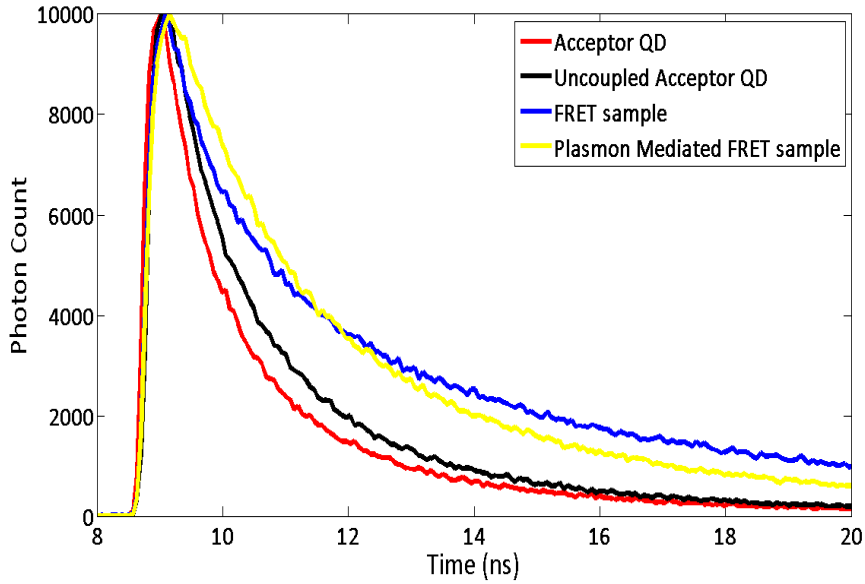

Figure 4. 14 TRF spectra of our acceptor and plasmon mediated FRET samples.

Figure 4.15 shows the decay lifetimes of the donor nanocrystals for four different cases: in individual nanocrystal sample, in only plasmon coupled sample, in FRET sample and finally in plasmon mediated FRET sample. The decay lifetime of the donor nanocrystals is shortened from 1.33 ns to 0.43 ns in the presence of gold nanoparticles. This shows the strong coupling between the two particles. For the case of FRET sample, donor NC lifetime is also shortened and found to be 0.87 ns. This also shows the existence of energy transfer between donor and acceptor nanocrystals. Finally, in the case of plasmon mediated sample, the donor lifetime is further shortened and measured to be 0.25 ns. This observation shows the strong coupling between both the donor and acceptor nanocrystals as wells the donor and the gold nanoparticles.

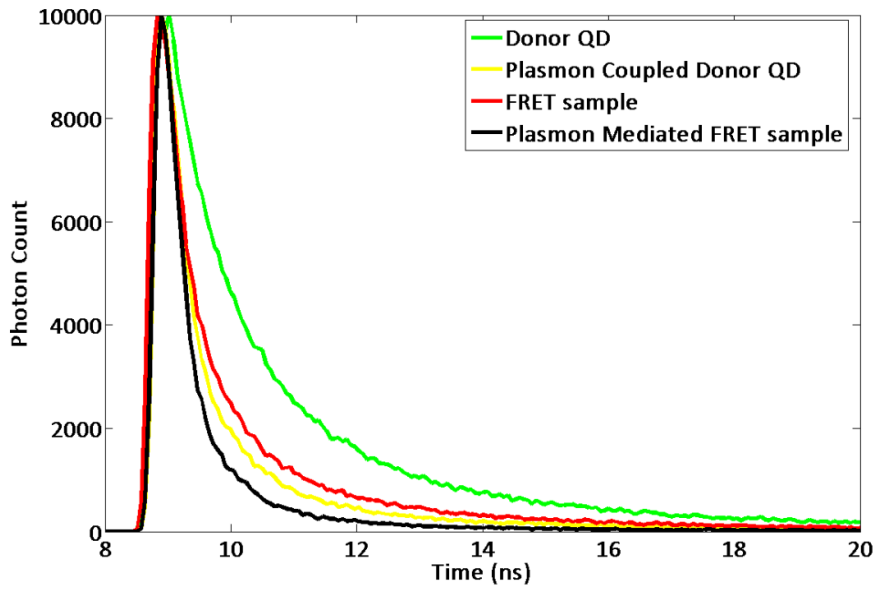

Figure 4. 15 TRF spectra of our only donor, FRET, uncoupled donor and plasmon mediated FRET samples.

We also studied the same architecture with different nanocrystals as the acceptor and donor pairs. CdTe colloidal quantum dots that have the peak emission wavelengths at 600 nm are chosen as the acceptor nanocrystals while CdTe colloidal quantum dots that have the emission peak wavelengths at 540 nm are chosen as the donor nanocrystals. In this case, the spectral overlap between the absorption spectrum of the acceptor nanocrystals and the emission spectrum of the donor nanocrystals becomes greater than that of the previous samples. In Figure 4.16, photoluminescence decay curves of the samples containing donor only, acceptor only, donor and acceptor together and finally all the particles including gold together are presented. The areas under these curves are calculated using trapezoidal fitting technique and normalized values are listed in Tables 4.1 and 4.2.

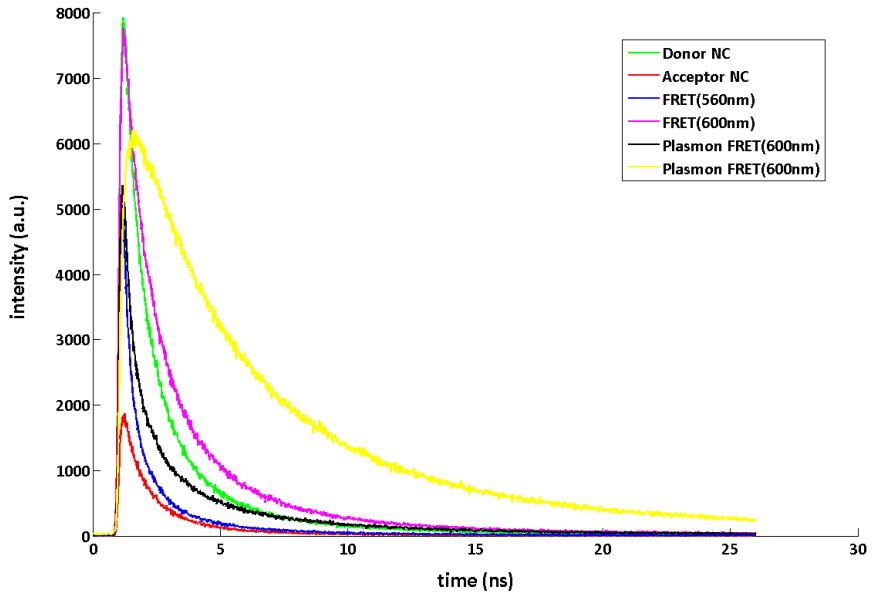

Figure 4. 16 TRF spectra of donor, acceptor, FRET and plasmon mediated FRET samples.

As can be seen in Figure 4.16, emission of the acceptor nanocrystals is increased compared to the samples containing the acceptor nanocrystals only and the acceptor and donor nanocrystals together. The emission enhancement of 6.5 folds is achieved, which is 3 times better than the sample of the same architecture but different nanocrystals. This is because of greater spectral overlap between these nanocrystals. This situation is even more striking in the case of the donor emission since the donor emission is quenched compared to the sample of weaker spectral overlap. Quenching is due to nonradiative energy transfer of the donor nanocrystals excitation energy to the acceptor nanocrystals.

Donor sample	FRET sample	Plasmon FRET sample
6.2	1.0	2.3

Table 4. 1 Integrated emission intensities at the peak wavelength of the donor nanocrystals.

Acceptor	FRET sample	Plasmon FRET sample
1	2.2	6.5

Table 4. 2 Integrated emission intensities at the peak emission wavelength of the acceptor nanocrystals.

In summary, we proposed and demonstrated cascading of plasmonic and nonradiative energy transfer interactions via plasmon-coupling selectively either to only donor NCs or to only acceptor NCs of the energy transfer pairs. This approach allowed us to control spatially plasmon-exciton interactions to take place distinctly either at the energy transfer starting site of donors or at the energy transfer finishing site of acceptors.

Chapter 5

Conclusions

In this thesis work, we studied both separate and combined effects of Förster and plasmon coupled non-radiative energy transfer mechanisms that are selectively cascaded and modified using spatial control of semiconductor quantum dots and metal nanoparticles in various layered architectures.

In this thesis, plasmon coupling mechanism between semiconductor quantum dots and metal nanoparticles is discussed after a background on electromagnetics of metals and plasmons is given. Theoretical explanation of distance dependent plasmon coupled energy transfer is provided and followed by the steady state and time resolved photoluminescence data analysis of our plasmon coupled quantum dots and negative control group quantum dots. Here we showed that plasmon coupling weakens for long distances while it enhances the energy transfer for a certain range of distances and quenches the emission of quantum dots for closer distances. In addition, Au nanoparticle synthesis is explained together with their size control using thin film deposition.

Following a brief introduction in utilization of quantum dots in optoelectronics, emission properties and decay lifetime of quantum dots are discussed in detail through the explanation of theory of quantum confined materials and analysis of optical characterization data. Here we showed that the peak emission wavelength of quantum dots shifts to longer wavelengths as their size grows.
Additionally, CdTe nanocrystal synthesis procedure is given along with the nanocrystal data provided for showing the size growth of quantum dots with increased time of synthesis.

Förster resonance energy transfer mechanism is discussed on a theoretical background and through data analysis of our thin film FRET samples. In FRET, we showed that, emission of larger nanocrystals can be enhanced via transferred excitation energy of smaller nanocrystals for certain separating distances between the particles. We demonstrated that plasmon mediated energy transfer can be achieved for both plasmon coupling to only donor or only acceptor quantum dots. We designed our samples in such a way that separate effects of both energy transfer mechanisms are revealed. For only donor plasmon coupled case energy is both transferred to metal nanoparticles and acceptor nanocrystals. Therefore, although FRET and plasmon coupling seem to work as competing mechanisms at first glance, they increased together the energy efficiency and rate from the donor nanocrystals to the acceptor nanocrystals. On the other hand for only acceptor plasmon coupled FRET case, the situation is relatively simpler since the excitation energy is transferred from acceptor nanocrystals to metal nanoparticles and returned via plasmon coupling and is not further transferred to donor nanocrystals. Also, excitation energy of donor are transferred to acceptor nanocrystals; thus, the emission of acceptor nanocrystals is further enhanced.

BIBLIOGRAPHY

[1] Eustis S, El-Sayed Ma. Why gold nanoparticles are more precious than pretty gold: noble metal surface plasmon resonance and its enhancement of the radiative and nonradiative properties of nanocrystals of different shapes. *Chemical Society reviews*. 2006;35(3):209-17.

[2] Pelton M, Aizpurua J, Bryant G. Metal-nanoparticle plasmonics. *Laser & Photonics Review*. 2008;2(3):136-159.

[3] Mie G, Considerations on the optic of turbid media, especially colloidal metal sols, *Ann. Phys.*, vol. 25, 1908, pp. 377-442.

[4] Ritchie R.H. Plasma Losses by Fast Electrons in Thin Films. *Physical Review;* 1957:1-8.

[5] Fano U, The theory of anomalous diffraction gratings and of quasi-stationary waves on metallic surfaces (Sommerfeld's waves)"*J.Opt.Soc.Am*.,31:213-222

[6] Hutter E, Fendler JH. Exploitation of Localized Surface Plasmon Resonance. *Advanced Materials*. 2004;16(19):1685-1706.

[7] Alivisatos P. The use of nanocrystals in biological detection. *Nature biotechnology*. 2004;22(1):47-52.

[8] Alivisatos P. Perspectives on the Physical Chemistry of Semiconductor Nanocrystals. *The Journal of Physical Chemistry*. 1996;100(31):13226-13239.

[9] C. B. Murray, D. J. Norris, M. G. Bawendi, Synthesis and Characterization of Nearly Monodisperse CdE Semiconductor Nanocrystallites. *J. Am. Chem. Soc.* 115(19):8706-8715 [1993]

[10] Hines Ma, Guyot-Sionnest P. Synthesis and Characterization of Strongly Luminescing ZnS-Capped CdSe Nanocrystals. *The Journal of Physical Chemistry*. 1996;100(2):468-471.

[11] Nizamoglu S, Akin O, Demir HV. Quantum efficiency enhancement in nanocrystals using nonradiative energy transfer with optimized donor-acceptor ratio for hybrid LEDs. *Applied Physics Letters*. 2009;94(24):243107.

[12] Gur I, Fromer Na, Chen C, Kanaras AG, Alivisatos aP. Hybrid solar cells with prescribed nanoscale morphologies based on hyperbranched semiconductor nanocrystals. *Nano letters*. 2007;7(2):409-14. Available at: http://www.ncbi.nlm.nih.gov/pubmed/17298008.

[13] T. Förster, "Zwischenmolekulare Energiewanderung und Fluoreszenz," *Ann. Physik,* vol. 437, 1948, pp. 55-75.

[14] Gersten J. *Accelerated energy transfer between molecules near a solid particle*.; Chem. Phys. Lett. 1984 104,1:31-37.

[15] Cheng M, Liu S, Zhou H, Hao Z, Wang Q. Coherent exciton-plasmon interaction in the hybrid semiconductor quantum dot and metal nanoparticle complex. *Optics letters*. 2007;32(15):2125-7.

[16] Wang CH, Chen CW, Chen YT, Surface plasmon enhanced energy transfer between type I CdSe/ZnS and type II CdSe/ZnTe quantum dots. *Applied Physics Letters*. 2010;96(7):071906.

[17] C. A. Balanis, *Advanced Engineering Electromagnetics*, John Wiley & Sons Publishing Corporation, 1989.

[18] N. W. Ashcroft and N. D. Mermin, *Solid State Physics*, Harcourt College Publishers, 1976.

[19] L. D. Landau and E. M. Fifshitz, *Electrodynamics of Continuous Media*, 2nd Edition, Pergamon Press, 1984.

[20] E.M. Purcell, Resonance Absorption by Nuclear Magnetic Moments in a Solid, Phys. Rev. 69, 681 (1946).

[21] Thomas M, Greffet J, Carminati R, Arias-Gonzalez JR. Single-molecule spontaneous emission close to absorbing nanostructures. *Applied Physics Letters*. 2004;85(17):3863.

[22] Anger P, Bharadwaj P, Novotny L. Enhancement and Quenching of Single-Molecule Fluorescence. *Physical Review Letters*. 2006;96(11):3-6.

[23] Cheng M, Liu S, Zhou H, Hao Z, Wang Q. Coherent exciton-plasmon interaction in the hybrid semiconductor quantum dot and metal nanoparticle complex. *Optics letters*. 2007;32(15):2125-7.

[24] Govorov AO, Bryant GW, Zhang W, et al. Exciton−Plasmon Interaction and Hybrid Excitons in Semiconductor−Metal Nanoparticle Assemblies. *Nano Letters*. 2006;6(5):984-994.

[25] Yan J, Zhang W, Duan S, Zhao X, Govorov A. Optical properties of coupled metal-semiconductor and metal-molecule nanocrystal complexes: Role of multipole effects. *Physical Review B*. 2008;77(16):1-9.

[26] C. Murray, B. Kagan, M. Bawendi Synthesis and Characterization of Monodisperse Nanocrystals and Close-packed Nanocrystal Assemblies Annu. Rev. Matter. Sci. 30:545-610 (2000)

[27] Saleh E.A., Fundamentals of photonics, Wiley-Interscience; 1 edition (1991)

[28] Klimov V., Semiconductor and Metal Nanocrystals: Synthesis and Electronic and Optical Properties (Optical Science and Engineering), CRC Press; 1 edition (2003)

[29] Gammon D. and Steel D., Optical Studies of Single Quantum Dots, Physics Today, 14, 36-41 (2002)

[30] Yin Y, Alivisatos aP. Colloidal nanocrystal synthesis and the organic-inorganic interface. *Nature*. 2005;437(7059):664-70.

[31] Cushing, B. L., Kolesnichenko, V. L. & O'Connor, C. J. Recent advances in the liquid-phase syntheses of inorganic nanoparticles. Chem. Rev. 104, 3893–3946 (2004).

[32] Pileni, M. P. The role of soft colloidal templates in controlling the size and shape of inorganic nanocrystals. Nature Mater. 2, 145–150 (2003).

[33] W.W. Yu et al. Chem. Matter, 15 2854-2860 (2003)

[34] S. V. Gaponenko, *Optical Properties of Semiconductor Nanocrystals*, Cambridge University Press, 2005.

[35] K.B.Blodgett. J. Am. Chem. Soc. 56, 495 (1934)

[36] Decher G. Fuzzy Nanoassemblies: Toward Layered Polymeric Multicomposites. *Science*. 1997;277(5330):1232-1237.

[37] Reilly RS, Smyth Ca, Rakovich YP, McCabe EM. The photoluminescent lifetime of polyelectrolytes in thin films formed via layer by layer self-assembly. *Nanotechnology*. 2009;20(9):095707.

[38] Dubas ST, Schlenoff JB. Swelling and Smoothing of Polyelectrolyte Multilayers by Salt. *Society*. 2001;(11):7725-7727.

[39] Matsuda K, Ito Y, Kanemitsu Y. Photoluminescence enhancement and quenching of single CdSe⁄ZnS nanocrystals on metal surfaces dominated by plasmon resonant energy transfer. *Applied Physics Letters*. 2008;92(21):211911.

[40] Komarala VK, Bradley aL, Rakovich YP, et al. Surface plasmon enhanced Förster resonance energy transfer between the CdTe quantum dots.

[41] Wang C., Chen C., Chen Y., Surface plasmon enhanced energy transfer between type I CdSe/ZnS and type II CdSe/ZnTe quantum dots. *Applied Physics Letters*. 2010;96(7):071906.

[42] Lakowicz J, Fu Y. Modification of single molecule fluorescence near metallic nanostructures. *Laser & Photonics Review*. 2009;3(1-2):221-232.

[43] Kulakovich O, Strekal N, Yaroshevich A, et al. Enhanced Luminescence of CdSe Quantum Dots on Gold Colloids. *Nano Letters*. 2002;2(12):1449-1452.